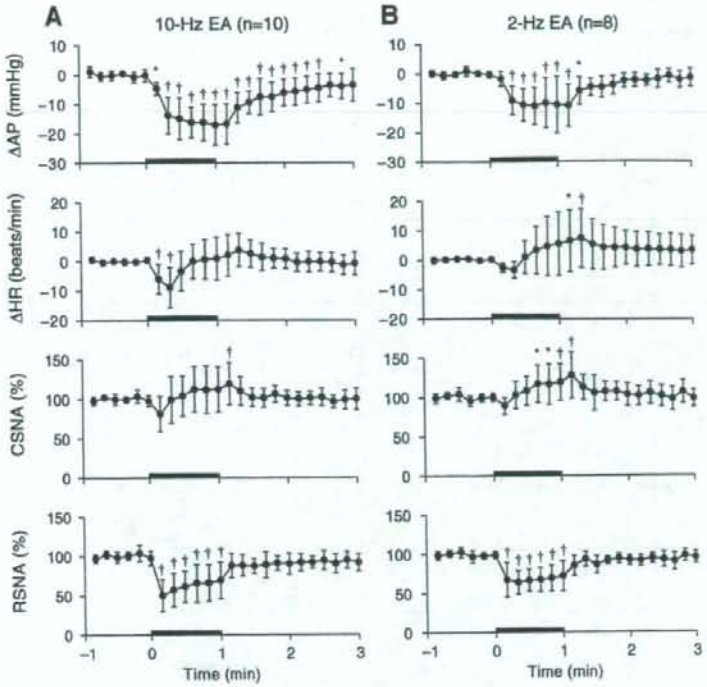

Fig. 2. Changes in arterial pressure (ΔAP), changes in heart rate (ΔHR), percent values of cardiac sympathetic nerve activity (CSNA), and percent values of renal sympathetic nerve activity (RSNA) during 10-Hz electroacupuncture (EA) (A) and 2-Hz EA (B) averaged for all trials. Values are the mean±SD. *$P<0.05$ and †$P<0.01$ from the first data point during the pre-EA baseline period.

RSNA were expected to be decreased by phenylephrine-induced hypertension.

2.4. Data analysis

Data were digitized by a 16-bit analog-to-digital converter (Contec, Japan) and stored at 200 Hz in a dedicated laboratory computer system. Because the absolute voltage of nerve activity varied among animals depending on the recording conditions, we normalized the nerve activity by a 1-min averaged value during the baseline condition before applying stimulation. The minimal inter-burst activity of the nerve signal was treated as the zero level. To examine changes in AP, HR, CSNA, and RSNA, we used 10-s averaged data. The data were analyzed using repeated-measures one-way analysis of variance (ANOVA) followed by Dunnett's test (Glantz, 2002). The first data point of the baseline condition was treated as the control. To analyze the correlation between changes in AP and CSNA or RSNA, that between changes in AP and changes in HR, and that between CSNA and RSNA, we performed a linear regression analysis between the two variables (Glantz, 2002). To analyze the correlation between changes in HR and CSNA or RSNA, we first fit the relationship to the following equation using a nonlinear least square fitting (a downhill simplex method) (Nelder and Mead, 1965).

$$y = \text{slope} \times \log_{10}(\text{offset} + x) + \text{intercept}$$

where x and y represent changes in HR and sympathetic nerve activity, respectively. After determining the optimal offset value for x, an ordinary linear regression analysis was performed between $[\log_{10}(\text{offset}+x)]$ and y to examine the significance of the slope. In all of the regression analyses, the correlation was considered significant when the slope was significantly different from zero. We used paired-t test to examine the difference between the CSNA and RSNA during the time period of maximum AP elevation induced by phenylephrine in Protocol 4. To examine the difference in the initial HR response to 10-Hz EA between Protocols 1 and 3, we used unpaired-t test because the number of trials was different between Protocols 1 and 3. The differences were considered significant at $P<0.05$.

3. Results

Typical recordings of 10-Hz EA obtained from two different cats are shown in Fig. 1. Horizontal arrows above the top panels indicate the period of EA. In one animal (Fig. 1A), AP was decreased by EA. HR decreased initially but increased from approximately 20 s after the onset of EA. As can be seen in the 2-s moving averaged signal (m-CSNA), CSNA exhibited changes similar to HR, i.e., it decreased at the onset of EA but gradually increased above the baseline level during the later portion of 1-min EA. RSNA and its 2-s moving averaged signal (m-RSNA) decreased at the onset of EA and gradually returned toward the baseline level. In another animal (Fig. 1B), both AP and HR were decreased by EA. Both CSNA and RSNA were also suppressed during EA, but the magnitude of suppression was greater in RSNA than in CSNA. Among the 5 animals, three showed the former type of AP and HR responses and remaining two showed the latter type. The type of AP and HR responses was consistent in each animal, i.e., the observed difference depended on the animal rather than the trial.

Fig. 2A summarizes changes in AP, HR, CSNA, and RSNA in response to 10-Hz EA. We performed EA trials in the left and right hind limbs in each animal and pooled data for 10 trials from 5 animals because there did not appear to be significant laterality in the effects of EA. The thick line on the abscissa in each panel indicates the period of EA. Baseline AP and HR values were 101±17 mmHg and 161±24 beats/min, respectively. AP was significantly decreased by EA and the decrease lasted over 1 min after

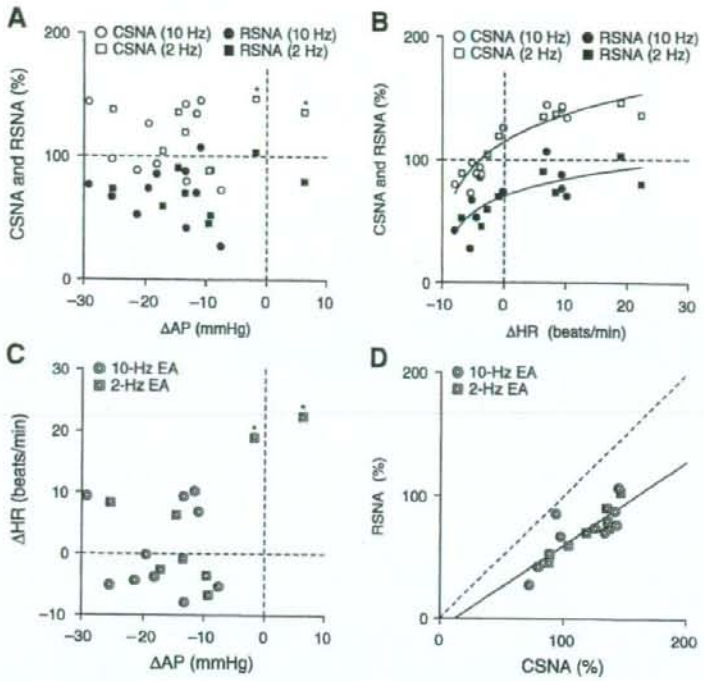

Fig. 3. Scatter plots of data obtained from the last 10 s of 1-min electroacupuncture (EA). A: Percent values of cardiac sympathetic nerve activity (CSNA) and renal sympathetic nerve activity (RSNA) plotted against changes in arterial pressure (ΔAP). Open and closed circles indicate CSNA and RSNA during 10-Hz EA, respectively. Open and closed squares indicate CSNA and RSNA during 2-Hz EA, respectively. Open squares with asterisks indicate data points where CSNA increased during EA even when AP did not decrease significantly or even increased. There was no significant relationship between changes in AP and CSNA ($r^2=0.0025$, $P=0.84$) or RSNA ($r^2=0.0039$, $P=0.81$). B: CSNA and RSNA plotted against changes in heart rate (ΔHR). Positive curvilinear relationships were observed between ΔHR and CSNA [$CSNA=83.0\times\log_{10}(11.5+\Delta HR)+26.7$, $r^2=0.86$, $P<0.01$] and between ΔHR and RSNA [$RSNA=46.6\times\log_{10}(10.1+\Delta HR)+23.6$, $r^2=0.56$, $P<0.01$]. C: Scatter plots of ΔHR versus ΔAP during 10-Hz EA (double circles) and 2-Hz EA (double squares). Except for the two data points with asterisks, there was no apparent relationship between changes in AP and those in HR ($r^2=0.17$, $P=0.094$ when the points with asterisk were included; $r^2=0.048$, $P=0.41$ when the points with asterisk were excluded). D: Scatter plots of RSNA versus CSNA during 10-Hz EA (double circles) and 2-Hz EA (double squares). There was a quasi-linear relationship between RSNA and CSNA ($RSNA=0.69\times CSNA-8.8$, $r^2=0.71$, $P<0.01$). The dashed line indicates the line of identity.

the cessation of EA. HR was significantly decreased in the first 20 s of EA but returned to the baseline level thereafter while EA continued. There was large variance in the CSNA response to EA among animals. Only the increase in CSNA after the cessation of EA was statistically significant. In contrast, RSNA was significantly decreased by EA during the entire period of EA.

Fig. 2B summarizes changes in AP, HR, CSNA, and RSNA in response to 2-Hz EA. We pooled data for 8 trials from 4 animals (left and right trials in each animal). Baseline AP and HR values were 98±17 mmHg and 151±20 beats/min, respectively. AP was decreased by EA, but the decrease was smaller and the duration of post-EA hypotension shorter than those observed in 10-Hz EA. HR increased with large variance during EA, and the increase was statistically significant after the cessation of EA. CSNA increased during the last 30 s of EA and remained increased for approximately 10 s after the cessation of EA. RSNA was decreased by EA during the period of EA, but the decrease appeared to be smaller than that observed with 10-Hz EA.

Fig. 3 illustrates scatter plots of data obtained during the last 10 s of EA. Because changes in AP nearly reached the steady state during the last 10 s of EA (Fig. 2A and B), we focused on these data. Open and closed circles in Fig. 3A and B indicates CSNA and RSNA data obtained from 10-Hz EA, respectively. Open and closed squares indicate CSNA and RSNA data obtained from 2-Hz EA, respectively. There was no apparent relationship between changes in AP and CSNA ($r^2=0.0025$, $P=0.84$) or RSNA ($r^2=0.0039$, $P=0.81$) by a linear regression analysis (Fig. 3A). In contrast, a positive curvilinear relationship was observed between changes in HR and CSNA [$CSNA=83.0\times\log_{10}(11.5+\Delta HR)+26.7$, $r^2=0.86$, $P<0.01$] or RSNA [$RSNA=46.6\times\log_{10}(10.1+\Delta HR)+23.6$, $r^2=0.56$, $P<0.01$] (Fig. 3B). Double circles and squares in Fig. 3C and D indicate data obtained from 10-Hz EA and 2-Hz EA, respectively. In Fig. 3C, the two data points with asterisks indicate that 2-Hz EA increased HR by approximately 20 beats/min when changes in AP were close to zero or positive. However, except for the two data points, there was no apparent relationship between changes in AP and changes in HR ($r^2=0.17$, $P=0.094$ when the points with asterisk were included; $r^2=0.048$, $P=0.41$ when the points with asterisk were excluded). As indicated by Fig. 3A and B, the RSNA values were lower than the corresponding CSNA data (Fig. 3D), though CSNA and RSNA were both normalized to 100% during the baseline condition. A linear regression analysis revealed a significant positive correlation between CSNA and RSNA during the last 10 s of EA ($RSNA=0.69\times CSNA-8.8$, $r^2=0.71$, $P<0.01$).

As shown in Fig. 4A, there were no significant changes in AP, HR, CSNA, or RSNA during stimulation applied to a control point in the front of the right thigh. Baseline AP and HR values were 92±15 mmHg and 158±16 beats/min, respectively.

After sinoaortic denervation and vagotomy, baseline AP and HR values were 120±25 mmHg and 184±19 beats/min, respectively. As shown in Fig. 4B, 10-Hz EA decreased AP by approximately 30 mmHg. AP returned gradually to the pre-EA value after the cessation of EA. HR decreased slightly from 20 to 30 s and returned to the pre-EA baseline value thereafter. CSNA decreased only at the onset of EA. After the cessation of EA, CSNA exhibited a slight increase for approximately 20 s. RSNA decreased at the onset of EA. Although the magnitude of RSNA decrease became smaller with time, RSNA remained decreased during the period of EA.

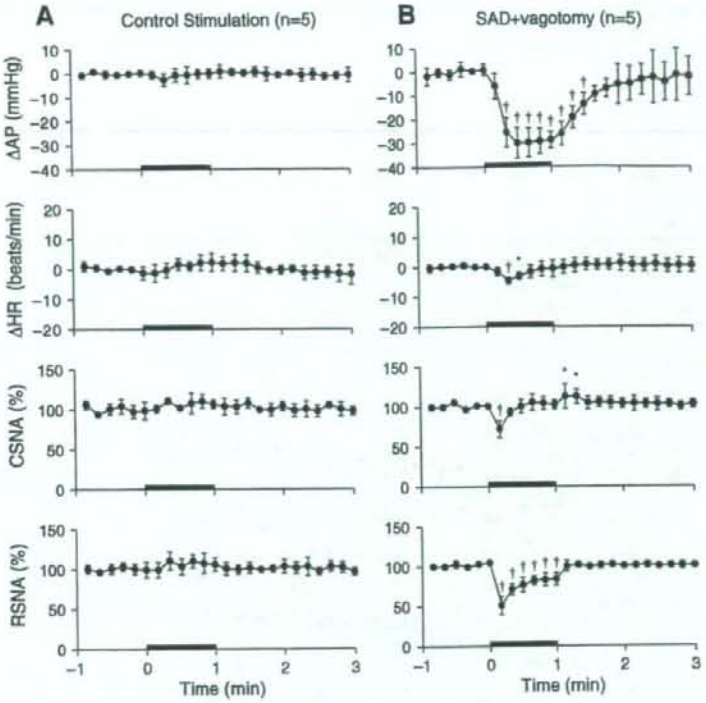

Fig. 4. Changes in arterial pressure (ΔAP), changes in heart rate (ΔHR), percent values of cardiac sympathetic nerve activity (CSNA), and percent values of renal sympathetic nerve activity (RSNA) during electrical stimulation at a nonspecific control point (A) and 10-Hz electroacupuncture (EA) after sinoaortic denervation (SAD) and vagotomy (B) averaged for all trials. Values are the mean±SD. *$P<0.05$ and †$P<0.01$ from the first data point during pre-EA baseline period.

Fig. 5A depicts changes in AP, HR, CSNA, and RSNA induced by intravenous bolus injection of phenylephrine (5 μg/kg). The data were obtained before sinoaortic denervation and vagotomy. Baseline AP and HR values were 98±24 mmHg and 163±30 beats/min, respectively. As expected, phenylephrine increased AP but decreased HR. Both CSNA and RSNA were decreased by phenylephrine injection. The suppression of CSNA persisted longer than that of RSNA. There was no significant correlation between CSNA and RSNA during the baseline condition immediately before the administration of phenylephrine (Fig. 5B, white circles, $r^2=0.32$, $P=0.32$). When CSNA and RSNA were compared during the time period of phenylephrine-induced maximum AP elevation, there was no significant correlation either (Fig. 5B, filled circles, $r^2=0.0003$, $P=0.98$).

4. Discussion

We have demonstrated that CSNA and RSNA responded differentially to EA applied to a hind limb in pentobarbital-anesthetized cats. Although the CSNA and RSNA responses were discordant, we found that CSNA and RSNA attained a new linear relationship during the last 10 s of EA (Fig. 3D), regardless of the stimulus frequency of EA.

4.1. Effects of EA on CSNA and RSNA

The neural mechanisms underlying hemodynamic responses to acupuncture are not fully understood. Recently, Uchida et al. (2007) demonstrated that manual acupuncture-like stimulation of a hind limb decreased CSNA and HR in pentobarbital-anesthetized rats. Their results complement the study by Ohsawa et al. (1995) showing that manual acupuncture-like stimulation decreased RSNA and AP. Although these results suggest that manual acupuncture-like stimulation causes systemic sympathoinhibition, we noted that HR did not necessarily decrease even when EA produced hypotensive effects in pentobarbital-anesthetized cats (Figs. 1A and 2A and B). Simultaneous recordings of CSNA and RSNA in the present study clearly supported the hypothesis that EA evoked regional differences among sympathetic nerve activities. Fig. 1A is a typical case in which CSNA increased without an associated increase in RSNA during the later portion of EA. In Protocol 2, no significant changes were observed (Fig. 4A), suggesting that hemodynamic and sympathetic nerve activity responses observed in Protocol 1 were not nonspecific responses to electrical stimulation. This does not mean, however, the point below the knee joint just lateral to the tibia (corresponding to an ST36 acupoint in humans) is the only specific point to produce cardiovascular responses. For instance, EA at the forelimb (corresponding to a PC6 acupoint in humans) exerts the cardiovascular effects in rats (Lujan et al., 2007).

Averaged data for 10-Hz EA (Fig. 2A) revealed a discrepancy between the CSNA and RSNA responses to EA. Both sympathoinhibition and sympathoexcitation appear to have occurred in CSNA during EA. We suspected that strong electrical stimulation might have caused nociceptive sympathoexcitatory responses in CSNA. However, reducing the stimulus frequency from 10 to 2 Hz resulted in a more pronounced excitatory response in CSNA during the later period of 1-min EA (Fig. 2B), suggesting that the increase in CSNA during EA was not a nociceptive response. Another factor that should be taken into account is effects of anesthesia. Matsukawa et al. (Matsukawa et al., 1993) demonstrated that sympathoinhibition induced by acute intravenous pentobarbital administration was larger and lasted longer in the case of CSNA than in that of RSNA in cats. The sympathoinhibitory response to EA may be easily observed when the baseline sympathetic tone is high. Because baseline sympathetic tone was probably lower in CSNA than in RSNA due to the pentobarbital anesthesia, the sympathoinhibitory response in CSNA might have been masked or hard to observe.

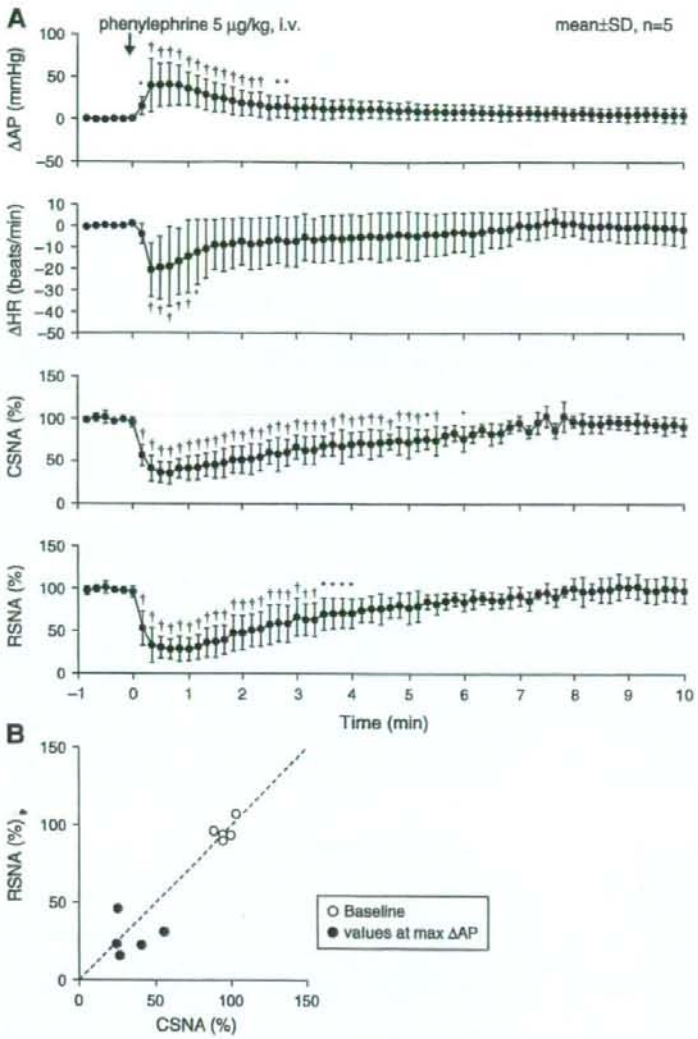

Fig. 5. A: Changes in arterial pressure (ΔAP), changes in heart rate (ΔHR), percent values of cardiac sympathetic nerve activity (CSNA), and percent values of renal sympathetic nerve activity (RSNA) during intravenous bolus injection of phenylephrine (5 μg/kg). Values are the mean±SD. *$P<0.05$ and †$P<0.01$ from the first data point during the baseline period. B: Scatter plots between CSNA and RSNA during the baseline condition immediately before the administration of phenylephrine (white circles) and those during the time period of phenylephrine-induced maximum AP elevation (filled circles). There was no significant correlation between CSNA and RSNA. The dashed line indicates the line of identity.

Although we measured left CSNA near the ventral ansa of the left stellate ganglion, there are several connections between the vagal and sympathetic nerves to form the cardiopulmonary nerves (Armour and Hopkins, 1984). Because we did not cut the vagi at the neck in Protocols 1 and 2, possibility of vagal contamination in the CSNA recording cannot be ruled out. However, because phenylephrine-induced hypertension that can increase vagal efferent activity (Kawada et al., 2001) attenuated CSNA to a similar degree to RSNA during the time period of maximum AP elevation (38.5±13.4% vs. 28.6±10.5%, $P=0.32$ by paired-t test, Fig. 5A), the effect of vagal contamination might have been a limited one.

4.2. Mechanistic considerations

In the present experimental settings, CSNA and RSNA exhibited decreasing responses to arterial baroreflex activation as demonstrated in previous studies (Fig. 5) (Minisi et al., 1989; Ninomiya et al., 1971), confirming that what we measured as CSNA and RSNA represented efferent sympathetic nerve activities. Because EA caused hypotension, it could exert sympathoexcitatory effects through the arterial baroreflex in Protocol 1. If the baroreflex-mediated sympathoexcitatory effect is stronger for CSNA than for RSNA, this may account for the discrepancy between the CSNA and RSNA responses. However, in some trials, CSNA was increased even when AP did not decrease sizably or was even increased (Fig. 3A, open squares with asterisks), suggesting that the baroreflex-medicated sympathoexcitatory effect cannot explain the increase in CSNA. Actually, the discrepancy between the CSNA and RSNA responses to 10-Hz EA persisted after sinoaortic denervation and vagotomy (Fig. 4B). Therefore, CSNA might have been activated in the later period of EA via mechanisms other than baroreflexes. This interpretation is in line with the conclusion by Sato et al. (1981) that variable changes in HR in response to somatic afferent stimulation were not an indirect consequence of preceding changes in blood pressure.

Although electrical stimulation of groups I and II muscle nerves of fore and hind limbs was not effective in changing HR (McCloskey and Mitchell, 1972; Sato et al., 1981), additional stimulation of group III nerves induced either tachycardia or bradycardia in anesthetized cats (Khayutin et al., 1986; Sato et al., 1981). Further, additional stimulation of group IV muscle nerves of a hind limb always produced tachycardia (Johansson, 1962; Tibes, 1977), with an optimal frequency between 6 and 15 Hz (Sato et al., 1981). In the present study, activation of group IV muscle nerves unlikely explain the tachycardiac response, since reducing the stimulus frequency from 10 to 2 Hz did not attenuate the tachycardiac response. Although Sato et al. (1981) concluded that whether group III muscle afferent stimulation induces tachycardia or bradycardia was difficult to predict, we found that there was a quasi-linear relationship between RSNA and CSNA during the last 10 s of 1-min EA, regardless of the stimulus frequency (Fig. 3D). When the sympathoinhibition assessed by RSNA was strong enough, CSNA decreased during EA. When the sympathoinhibition assessed by RSNA was weak, CSNA increased.

4.3. Limitations

Several limitations need to be addressed. First, we performed experiments under pentobarbital anesthesia. Our results might have differed had we used different anesthesia or performed the experiments in conscious animals. However, Sato et al. (1981) used chloralose and urethane anesthesia and reported divergence of HR responses induced by group III muscle fiber afferent stimulation. Therefore, the differences between CSNA and RSNA might not be explained by type of anesthesia alone.

Second, we measured only CSNA and RSNA. Changes in AP did not correlate with CSNA or RSNA (Fig. 3A), suggesting that the AP response to EA was not explained by changes in CSNA or RSNA. The abdominal vascular bed plays a significant role in the arterial blood pressure control (Rowell, 1974). Further studies such as that recording splanchnic nerve activity are needed to elucidate the total picture of the sympathetic mechanism for the AP response to EA.

Third, we did not perform vagotomy independently of sinoaortic denervation. Accordingly, the contribution of vagal nerve activity to the HR response was not identified. Comparing Figs. 2A and 4B, the initial drop in HR was much clearer before sinoaortic denervation and vagotomy ($P=0.025$ during the first 10 s after EA initiation by unpaired-t test) despite the similar profile of CSNA response to EA. Therefore, the vagal nerve activity might have contributed to the initial drop in HR in response to EA.

4.4. Conclusion

We demonstrated that EA evoked regional differences between CSNA and RSNA in pentobarbital-anesthetized cats. The differences persisted after sinoaortic denervation and vagotomy, suggesting the baroreflex-mediated sympathoexcitatory mechanisms alone cannot explain the discrepancy between CSNA and RSNA responses during EA. Although the responses were discordant, there was a linear relationship that persisted between CSNA and RSNA during the last 10 s of 1-min EA, suggesting that EA changes the relationship between CSNA and RSNA.

Acknowledgments

This study was supported by a "Health and Labour Sciences Research Grant for Research on Advanced Medical Technology", "Health and Labour Sciences Research Grant for Research on Medical Devices for Analyzing, Supporting, and Substituting the Function of the Human Body", and a "Health and Labour Sciences Research Grant (H18-Iryo-Ippan-023) (H18-Nano-Ippan-003)", from the Ministry of Health, Labour, and Welfare of Japan, the "Industrial Technology Research Grant Program" of the New Energy and Industrial Technology Development Organization of Japan.

References

Armour, J.A., Hopkins, D.A., 1984. Anatomy of the extrinsic efferent autonomic nerves and ganglia innervating the mammalian heart. In: Randall, W.C. (Ed.), Nervous Control of Cardiovascular Function. Oxford Univ. Press, New York, pp. 20–45.

DiBona, G.F., 2005. Physiology in perspective: the wisdom of the body. Neural control of the kidney. Am. J. Physiol., Regul. Integr. Comp. Physiol. 289 (3), R633–641.

Glantz, S.A., 2002. Primer of Biostatistics, 5th ed. McGraw-Hill, New York.

Johansson, B., 1962. Circulatory responses to stimulation of somatic afferents with special reference to depressor effects from muscle nerves. Acta Physiol. Scand., Suppl. 198, 1–91.

Kawada, T., Yamazaki, T., Akiyama, T., Shishido, T., Inagaki, M., Uemura, K., Miyamoto, T., Sugimachi, M., Takaki, H., Sunagawa, K., 2001. In vivo assessment of acetylcholine-releasing function at cardiac vagal nerve terminals. Am. J. Physiol. Heart Circ. Physiol. 281 (1), H139–145.

Kawada, T., Uemura, K., Kashihara, K., Jin, Y., Li, M., Zheng, C., Sugimachi, M., Sunagawa, K., 2003. Uniformity in dynamic baroreflex regulation of left and right cardiac sympathetic nerve activities. Am. J. Physiol., Regul. Integr. Comp. Physiol. 284 (6), R1506–1512.

Khayutin, V.M., Lukoshkova, E.V., Gailans, J.B., 1986. Somatic depressor reflexes: results of specific 'depressor' afferents' excitation or an epiphenomenon of general anesthesia and certain decerebrations? J. Auton. Nerv. Syst. 16 (1), 35–60.

Kimura, A., Sato, A., 1997. Somatic regulation of autonomic functions in anesthetized animals—neural mechanisms of physical therapy including acupuncture. Jpn. J. Vet. Res. 45 (3), 137–145.

Kline, R.L., Yeung, K.Y., Calaresu, F.R., 1978. Role of somatic nerves in the cardiovascular responses to stimulation of an acupuncture point in anesthetized rabbits. Exp. Neurol. 61 (3), 561–570.

Kobayashi, S., Noguchi, E., Ohsawa, H., Sato, Y., Nishijo, K., 1998. Experimental research on the reflex decrease of heart rate elicited by acupuncture stimulation in anesthetized rats (in Japanese). Jpn. Acupunct. Moxib. 48, 120–129.

Ku, Y.H., Zou, C.J., 1993. Tinggong (SI 19), a novel acupoint for 2 Hz electroacupuncture-induced depressor response. Acupunct. Electrother. Res. 18 (2), 89–96.

Lee, H.S., Kim, J.Y., 1994. Effects of acupuncture on blood pressure and plasma renin activity in two-kidney one clip Goldblatt hypertensive rats. Am. J. Chin. Med. 22 (3–4), 215–219.

Lin, M.C., Nahin, R., Gershwin, M.E., Longhurst, J.C., Wu, K.K., 2001. State of complementary and alternative medicine in cardiovascular, lung, and blood research: executive summary of a workshop. Circulation 103 (16), 2038–2041.

Lujan, H.L., Kramer, V.J., DiCarlo, S.E., 2007. Electroacupuncture decreases the susceptibility to ventricular tachycardia in conscious rats by reducing cardiac metabolic demand. Am. J. Physiol. Heart Circ. Physiol. 292 (5), H2550–H2555.

Matsukawa, K., Ninomiya, I., Nishiura, N., 1993. Effects of anesthesia on cardiac and renal sympathetic nerve activities and plasma catecholamines. Am. J. Physiol. 265 (4 Pt 2), R792–R797.

McCloskey, D.I., Mitchell, J.H., 1972. Reflex cardiovascular and respiratory responses originating in exercising muscle. J. Physiol. 224 (1), 173–186.

Minisi, A.J., Dibner-Dunlap, M., Thames, M.D., 1989. Vagal cardiopulmonary baroreflex activation during phenylephrine infusion. Am. J. Physiol. 257 (5 Pt 2), R1147–R1153.

Nelder, J.A., Mead, R., 1965. A simplex method for function minimization. Comput. J. 7, 308–313.

Ninomiya, I., Nisimaru, N., Irisawa, H., 1971. Sympathetic nerve activity to the spleen, kidney, and heart in response to baroceptor input. Am. J. Physiol. 221 (5), 1346–1351.

Ohsawa, H., Okada, K., Nishijo, K., Sato, Y., 1995. Neural mechanism of depressor responses of arterial pressure elicited by acupuncture-like stimulation to a hindlimb in anesthetized rats. J. Auton. Nerv. Syst. 51 (1), 27–35.

Rowell, L.B., 1974. Human cardiovascular adjustments to exercise and thermal stress. Physiol. Rev. 54 (1), 75–159.

Sato, A., Sato, Y., Schmidt, R.F., 1981. Heart rate changes reflecting modifications of efferent cardiac sympathetic outflow by cutaneous and muscle afferent volleys. J. Auton. Nerv. Syst. 4 (3), 231–247.

Sato, A., Sato, Y., Suzuki, A., Uchida, S., 1994. Reflex modulation of gastric and vesical function by acupuncture-like stimulation in anesthetized rats. Biomed. Res. 15, 59–65.

Sato, A., Sato, Y., Uchida, S., 2002. Reflex modulation of visceral functions by acupuncture-like stimulation in anesthetized rats. Int. Congr. Ser. 1238, 111–123.

Tibes, U., 1977. Reflex inputs to the cardiovascular and respiratory centers from dynamically working canine muscles. Some evidence for involvement of group III or IV nerve fibers. Circ. Res. 41 (3), 332–341.

Uchida, S., Shimura, M., Ohsawa, H., Suzuki, A., 2007. Neural mechanism of bradycardiac responses elicited by acupuncture-like stimulation to a hind limb in anesthetized rats. J. Physiol. Sci. 57 (6), 377–382.

Yasunaga, K., Nosaka, S., 1979. Cardiac sympathetic nerves in rats: anatomical and functional features. Jpn. J. Physiol. 29 (6), 691–705.

Zhou, W., Fu, L.W., Tjen, A.L.S.C., Li, P., Longhurst, J.C., 2005. Afferent mechanisms underlying stimulation modality-related modulation of acupuncture-related cardiovascular responses. J. Appl. Physiol. 98 (3), 872–880.

Annals of Biomedical Engineering, Vol. 37, No. 1, January 2009 (© 2008) pp. 82–93
DOI: 10.1007/s10439-008-9595-8

Computationally Managed Bradycardia Improved Cardiac Energetics While Restoring Normal Hemodynamics in Heart Failure

KAZUNORI UEMURA,[1] KENJI SUNAGAWA,[2] and MASARU SUGIMACHI[1]

[1]Department of Cardiovascular Dynamics, Advanced Medical Engineering Center, National Cardiovascular Center Research Institute, 5-7-1 Fujishirodai, Suita 565-8565, Japan; and [2]Department of Cardiovascular Medicine, Kyushu University Graduate School of Medical Sciences, Fukuoka 812-8582, Japan

(Received 9 September 2008; accepted 29 October 2008; published online 12 November 2008)

Abstract—In acute heart failure, systemic arterial pressure (AP), cardiac output (CO), and left atrial pressure (P_{LA}) have to be controlled within acceptable ranges. Under this condition, cardiac energetic efficiency should also be improved. Theoretically, if heart rate (HR) is reduced while AP, CO, and P_{LA} are maintained by preserving the functional slope of left ventricular (LV) Starling's curve (S_L) with precisely increased LV end-systolic elastance (E_{es}), it is possible to improve cardiac energetic efficiency and reduce LV oxygen consumption per minute (MVO_2). We investigated whether this hemodynamics can be accomplished in acute heart failure using an automated hemodynamic regulator that we developed previously. In seven anesthetized dogs with acute heart failure ($CO < 70$ mL min^{-1} kg^{-1}, $P_{LA} > 15$ mmHg), the regulator simultaneously controlled S_L with dobutamine, systemic vascular resistance with nitroprusside and stressed blood volume with dextran or furosemide, thereby controlling AP, CO, and P_{LA}. Normal hemodynamics were restored and maintained (CO; 88 ± 3 mL min^{-1} kg^{-1}, P_{LA}; 10.9 ± 0.4 mmHg), even when zatebradine significantly reduced HR (−27 ± 3%). Following HR reduction, E_{es} increased (+34 ± 14%), LV mechanical efficiency (stroke work/oxygen consumption) increased (+22 ± 6%), and MVO_2 decreased (−17 ± 4%) significantly. In conclusion, in a canine acute heart failure model, computationally managed bradycardia improved cardiac energetic efficiency while restoring normal hemodynamic conditions.

Keywords—Ventricular oxygen consumption, Mechanical efficiency, Specific bradycardic agent.

INTRODUCTION

Systemic arterial pressure (AP), cardiac output (CO), and left atrial pressure (P_{LA}) are three major variables necessary to guarantee survival. In the management of patients with acute heart failure following myocardial infarction or cardiac surgery, these variables have to be controlled within acceptable ranges.[1] Since the failing heart is in a critical state of myocardial energetics,[19] improvement of cardiac energetic efficiency is also essential in the management of such patients. Therapeutic interventions that enhance cardiac energetic efficiency have proven to be beneficial with respect to long-term outcome.[20] Reduction of heart rate (HR) has been shown to improve cardiac energetic efficiency.[6,26] However, in the failing heart, reduction of HR alone may decrease CO, and compromise hemodynamics.[5,13]

We previously demonstrated that AP, CO, and P_{LA} are determined by a mechanical equilibrium of the functional slope of Starling's curve (S_L) for the left ventricle (LV), systemic vascular resistance (R), and stressed blood volume (V).[30–32] Conversely, S_L, R, and V can be calculated from AP, CO, and P_{LA}, indicating that a set of AP, CO, and P_{LA} values uniquely corresponds to a set of S_L, R, and V values. When HR is reduced, the three variables of AP, CO, and P_{LA} can only be maintained by increasing LV contractility (LV end-systolic elastance, E_{es}) to offset HR reduction and to preserve S_L (see *Theoretical analysis* in "Materials and Methods"). In this hemodynamics, total mechanical energy of LV contraction, which is indicated by LV pressure–volume area (PVA), also increases with HR reduction. Increases in both E_{es} and PVA elevate LV oxygen consumption per beat (BVO_2).[28,29] However, since the increase in the external work done by LV is greater than the increase in BVO_2, cardiac energetic efficiency is improved. Furthermore, LV oxygen consumption per minute (MVO_2) decreases because the reduction in HR is sufficient to compensate for the increase in BVO_2.

To realize the above hemodynamics (optimal hemodynamics) in patients with acute heart failure, AP, CO, and P_{LA} should be controlled under HR

Address correspondence to Kazunori Uemura, Department of Cardiovascular Dynamics, Advanced Medical Engineering Center, National Cardiovascular Center Research Institute, 5-7-1 Fujishirodai, Suita 565-8565, Japan. Electronic mail: kuemura@ri.ncvc.go.jp

reduction by regulating infusions of multiple cardiovascular drugs such as inotropes and vasodilators. However, the control process is difficult and time-consuming, since the responses of AP, CO, and P_{LA} to these drugs vary between patients and within patient over time, and the responses are interrelated.[9,23] We previously demonstrated that it is possible to control AP, CO, and P_{LA} stably and accurately by directly controlling S_L, R, and V with cardiovascular drugs, due to their mechanical equilibrium.[30] This strategy is feasible because the responses of S_L to inotropes, R to vasodilators, and V to volume expander or diuretics are relatively invariable.[30] Furthermore, these three input–output relations; namely, inotrope–S_L, vasodilator–R, and volume expanders/diuretics–V are effectively decoupled. We hypothesized that this approach would be especially efficacious in accomplishing optimal hemodynamics in acute heart failure. Under HR reduction, an excessive increase in E_{es} will compromise the cardiac energetic efficiency.[15] Therefore E_{es} should be increased to a precise level. This can be done through a tight control of the inotrope–S_L relation. Although inotropes also affect R or V,[3,7] these effects can easily be compensated by the vasodilator–R and volume expanders/diuretics–V relations.

The purpose of this study was to prove the hypothesis that direct control of S_L, R, and V under HR reduction attains the optimal hemodynamics and at the same time improves cardiac energetic efficiency and reduces MVO_2 in a canine model of acute heart failure, as predicted in *Theoretical Analysis*. An automated hemodynamic regulator that we developed previously[30] was used to directly control S_L, R, and V. The regulator directly controls S_L with dobutamine (DOB), R with sodium nitroprusside (SNP), and V with dextran (DEX) and furosemide (FUR), thereby controlling AP, CO, and P_{LA}. To reduce HR, we used a specific bradycardic agent, zatebradine (UL-FS49) that specifically reduces HR without affecting LV contractility.[12,24]

MATERIALS AND METHODS

Theoretical analysis

S_L is theoretically determined by E_{es}, HR, R, and diastolic myocardial stiffness (k), and can be expressed by the following formula[31]:

$$S_L = \frac{1}{k} \cdot \frac{E_{es}}{(E_{es}/HR) + R} \tag{1}$$

Equation (1) can be rewritten as follows:

$$E_{es} = \frac{S_L \cdot k \cdot R}{1 - S_L \cdot k/HR} \tag{2}$$

The external work done by LV is represented by stroke work (SW) and expressed as[11]

$$SW = (P_{es} - P_{ed}) \cdot CO/HR \tag{3}$$

where P_{es} is LV end-systolic pressure and P_{ed} is end-diastolic pressure. In the LV pressure–volume diagram, PVA is the area circumscribed by the end-systolic pressure volume relation, the end-diastolic pressure volume relation, and the systolic pressure volume trajectory of LV. PVA, an index of total mechanical energy of LV contraction, is the sum of potential energy and external work of LV,[28,29] and can be expressed as

$$PVA = P_{es} \cdot P_{es}/2E_{es} + SW \tag{4}$$

If we approximate P_{es} to AP and P_{ed} to P_{LA}, SW and PVA can be expressed as

$$SW = (AP - P_{LA}) \cdot CO/HR \tag{5}$$

$$PVA = AP \cdot AP/2E_{es} + SW \tag{6}$$

BVO_2 is related to PVA and E_{es} as follows[28,29]:

$$BVO_2 = \alpha \cdot PVA + \beta \cdot E_{es} + \gamma \tag{7}$$

where α, β, and γ are constants representing oxygen cost of PVA, oxygen cost of contractility, and basal metabolism, respectively. MVO_2 is expressed as follows:

$$MVO_2 = BVO_2 \cdot HR \tag{8}$$

Using Eqs. (2–8) and fixed values of AP, CO, and P_{LA} (Table 1), we numerically simulated the individual relations of HR with E_{es}, SW, PVA, BVO_2, LV mechanical efficiency (ME) and MVO_2 (Fig. 1). In these computations, representative k, α, β, and γ values (Table 1) were used, which are appropriate for a 20-kg dog.[10,29] In Eq. (2), S_L was calculated from the ratio of CO to logarithmic function of P_{LA} as described

TABLE 1. Values of the parameters used in *Theoretical Analysis*.

Parameters	Values
AP, mmHg	100
CO, mL min^{-1} kg^{-1}	100
P_{LA}, mmHg	10
k, mL^{-1}	0.082
α, mL O_2 · mmHg^{-1} · mL^{-1}	1.8×10^{-5}
β, mL O_2 · beat^{-1} · mmHg^{-1} · mL	0.0018
γ, mL O_2 · beat^{-1}	0.01

AP, systemic arterial pressure; CO, cardiac output; P_{LA}, left atrial pressure; k, left ventricular diastolic myocardial stiffness; α, oxygen cost of pressure–volume area; β, oxygen cost of contractility; γ, constant representing basal metabolism.

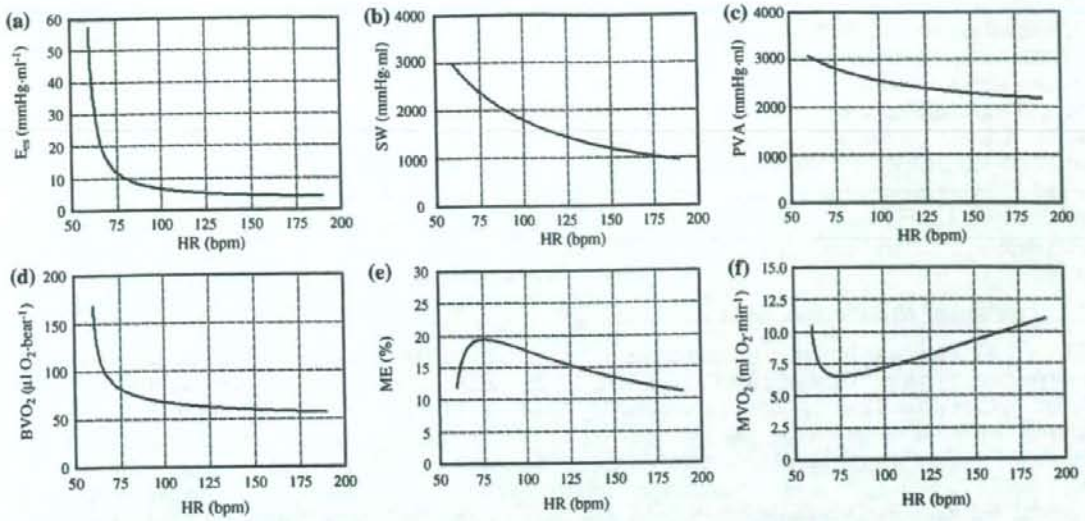

FIGURE 1. Simulated relations of heart rate (*HR*) with left ventricular end-systolic elastance (E_{es}) (a), left ventricular stroke work (*SW*) (b), left ventricular pressure–volume area (*PVA*) (c), left ventricular oxygen consumption per beat (BVO_2) (d), left ventricular mechanical efficiency (*ME*) (e), and left ventricular oxygen consumption per minute (MVO_2) (f), when systemic arterial pressure, cardiac output, and left atrial pressure are kept at fixed values. At *HR* of 75 bpm, *ME* becomes maximal (e), and MVO_2 becomes minimal (f).

previously.[30] R was calculated from the ratio of AP to CO. ME was calculated as the dimensionless ratio of SW to BVO_2.[19]

As indicated in Fig. 1, HR is inversely related to E_{es} (Fig. 1a), SW (Fig. 1b), PVA (Fig. 1c), and BVO_2 (Fig. 1d). Over the physiological range of HR for dogs (>80 bpm),[18] ME increases as HR is reduced (Fig. 1e) since SW increase is greater than BVO_2 increase; hence cardiac energetic efficiency is optimized. At HR of 75 bpm, ME becomes maximal and MVO_2 becomes minimal (Fig. 1f). When HR is reduced from 150 to 110 bpm, E_{es} increases from 4.6 to 5.9 mmHg mL^{-1} (29% increase) and ME increases from 13 to 17% (24% increase), whereas MVO_2 decreases from 8.9 to 7.2 mL O_2 min^{-1} (19% reduction). In addition to the simulation described above, we also simulated the relation of HR with MVO_2 for a variety of combinations of AP (80–120 mmHg), CO (80–100 mL min^{-1} kg^{-1}), and P_{LA} (10–20 mmHg). HR at which MVO_2 becomes minimal ranged from 50 to 75 bpm (data not shown). This indicates that as long as HR is within the physiological range, HR reduction together with compensatory increase of E_{es} consistently improves cardiac energetic efficiency and reduces MVO_2, irrespective of the target hemodynamics to be achieved.

Animal Preparation

After approval of the institutional Animal Care and Use Committee we studied 7 adult mongrel dogs (either sexes, 26 ± 4 kg). Anesthesia was induced with sodium pentobarbital (25 mg kg^{-1}). Animals were intubated endotracheally. Arterial pH, PO_2, and PCO_2 were maintained within the physiological ranges. Isoflurane (1.0%) was inhaled continuously during the experiment. After a median sternotomy and pericardial incision, an ultrasonic flow-meter (20A594, Transonics, Ithaca, NY) was placed around the ascending aorta to measure CO. Ultrasonic flow meters (2.5S273, Transonics, Ithaca, NY) were placed on the left circumflex and anterior descending coronary arteries to measure coronary blood flow. Fluid filled catheters were placed in the right femoral artery, left atrium and right atrium, and connected to pressure transducers (DX-200, Nihon Kohden, Tokyo, Japan) to measure AP, P_{LA}, and right atrial pressure, respectively. A catheter-tipped micromanometer (SPC-330A, Millar Instruments, Houston, TX) was introduced into the left ventricle to measure left ventricular pressure (LVP). A pair of pacing electrodes was fixed at the right atrial appendage for atrial pacing. A catheter (5F) was introduced into the coronary sinus via the right external jugular vein.

Two infusion pumps (CFV-3200, Nihon Kohden, Tokyo, Japan) for administering DOB and SNP, and a roller pump (Minipulse 3, Gilson, Middleton, WI) for administering DEX were attached to a catheter (5F) placed in the right femoral vein. These pumps were controlled with a laboratory computer (MA20V, NEC, Tokyo, Japan). From a catheter (5F) placed in the

right external jugular vein, FUR was injected following a command signal from the computer.

Analog signals of *AP*, *CO*, P_{LA}, right atrial pressure, LVP, and coronary blood flow were digitized (200 Hz, 12-bit) by the computer, and stored on a hard disk for off-line analysis. The digitized signals of *AP*, *CO*, and P_{LA} were smoothed by a low-pass filter with a time constant 10 s, and used as control variables for the regulator.

Automated Hemodynamic Regulator

Figure 2 is a schematic illustration of the automated hemodynamic regulator.[30] Once target values for *AP*, *CO*, and P_{LA} are defined and fed into the computer, it calculates the target values for S_L, *R*, and *V*. The subject's S_L, *R*, and *V* are calculated from the low-pass filtered *AP*, *CO*, and P_{LA} values. To minimize the differences between target and subject's S_L and *R*, proportional-integral feedback controllers adjust the infusion rates of DOB and SNP, respectively. To minimize the difference between target and subject's *V*, a nonlinear feedback controller adjusts the infusion of DEX or injection of FUR (see Appendix: Feedback control algorithms of the automatic hemodynamic regulator).

Experimental Protocols

After stabilization for 30 min, "baseline" hemodynamic data were recorded and blood samples were collected from the right femoral artery and the coronary sinus simultaneously for oxygen content determination (*Baseline*). Acute heart failure was induced by injecting glass microspheres (90 μm in diameter) to embolize the left circumflex coronary artery.[27] The amount of microspheres was adjusted to decrease *CO* to below 70 mL min^{-1} kg^{-1} or increase P_{LA} to above 15 mmHg. One hour after embolization, zatebradine (0.5 mg kg^{-1}) was administered intravenously to suppress the intrinsic atrial beat, and atrial pacing was then initiated to control *HR* at the level observed following coronary embolization. After the canine model of acute heart failure was established, hemodynamic measurements and blood sample collection were performed (*AHF*).

We activated the automated hemodynamic regulator with target values of 90–100 mmHg for *AP*, 80–100 mL kg^{-1} min^{-1} for *CO*, and 10–12 mmHg for P_{LA}. The regulator restored *AP*, *CO*, and P_{LA} to their respective target values within 30 min. After confirming stable hemodynamics, we collected blood samples as described above (*Initial HR*). We then reduced the pacing rate in steps of 10 or 20 bpm. The maximum *HR* reduction averaged 39 ± 12 bpm. For each *HR* step, we waited for hemodynamic stabilization, and then collected blood samples. After reaching the lowest HR (*Lowest HR*), we increased the *HR* stepwise back to the "Initial *HR*" to confirm the reproducibility of the hemodynamic control.

Data Analysis of LV Mechanoenergetics

We estimated E_{es} using a technique described previously.[14] In brief, the ratio of E_{es} to effective arterial elastance was estimated based on the fact that this ratio can be expressed as a function of P_{es}, LVP at which LV begins to eject, pre-ejection period, and

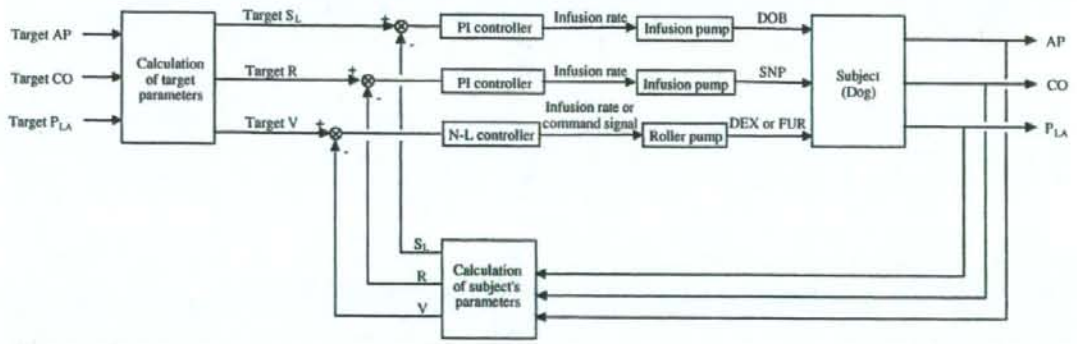

FIGURE 2. Schematic illustration of an automated hemodynamic regulator for simultaneous control of systemic arterial pressure (*AP*), cardiac output (*CO*), and left atrial pressure (P_{LA}). From target values of *AP*, *CO*, and P_{LA}, target values of functional slope of the left ventricular Starling's curve (S_L), systemic vascular resistance (*R*), and stressed blood volume (*V*) are determined. Subject's S_L, *V*, and *R* are calculated from low-pass filtered values of measured *AP*, *CO*, and P_{LA}. Proportional-integral (PI) feedback controllers adjust infusion rate of dobutamine (DOB) and sodium nitroprusside (SNP) to minimize the difference between target and subject's S_L and those of *R*, respectively. Nonlinear (N-L) feedback controller adjusts infusion of 10% dextran 40 (DEX) or injection of furosemide (FUR) to minimize the difference between target and subject's *V*.

ejection time. Effective arterial elastance is calculated as P_{es} divided by stroke volume. Therefore once we know the ratio, we can calculate E_{es}.[14] In this study, the end-diastolic point is defined as the moment when LV dP/dt exceeds 20% of positive dP/dt_{max}. The time point at which LV begins to eject is defined as the moment when the aortic flow begins. The end-systolic point is defined as the time when LV dP/dt decreases to 20% of LV dP/dt_{min}. Thus, pre-ejection period is obtained by subtracting the end-diastolic point from the time point at which LV begins to eject; and ejection time is obtained by subtracting the time point at which LV begins to eject from the end-systolic point.

SW was calculated using Eq. (3). *PVA* was calculated using Eq. (4). Oxygen contents of the blood samples were measured using a co-oxymeter (IL 682, Instrumentation Laboratory, Lexington, MA), and MVO_2 was calculated as the product of mean coronary blood flow and the coronary arteriovenous difference in oxygen content.[6] BVO_2 was calculated by dividing MVO_2 by *HR*. *ME* was calculated as described above.

Statistics

Group data are expressed as means ± SEM. Differences in hemodynamics, LV mechanoenergetics, and drug infusion rates among different conditions were evaluated using Student's paired *t*-test or a repeated-measures analysis of variance followed by Student-Newman–Keuls test. The level of statistical significance was defined as $p < 0.05$.

RESULTS

Hemodynamic and LV mechanoenergetic data at *Baseline* and *AHF* are summarized in Table 2. Coronary embolization nearly halved *CO* from 101 ± 5 to 62 ± 5 mL min^{-1} kg^{-1}, doubled P_{LA} from 8.9 ± 0.6 to 17.1 ± 0.7 mmHg, depressed E_{es} from 4.4 ± 0.7 to 2.5 ± 0.4 mmHg mL^{-1}, and halved MVO_2 from 5.8 ± 0.7 to 3.1 ± 0.2 mL min^{-1}. These changes are compatible with induction of acute ischemic heart failure.[27]

Figure 3 demonstrates the time courses of hemodynamics, the infusion rates of DOB and SNP, and the infused volume of DEX in a representative animal. Before activation of the regulator, *AP* was 108 mmHg, *CO* was 44 mL min^{-1} kg^{-1}, and P_{LA} was 16.9 mmHg. After activation of the regulator, the infusion rates of DOB, SNP, and DEX were adjusted automatically and S_L, *R*, and *V* reached their respective target values within 20 min. In this case, FUR was not used. By controlling S_L, *R*, and *V*, the regulator restored *AP*, *CO*, and P_{LA} to their respective target values (*AP*, 100 mmHg; *CO*, 80 mL min^{-1} kg^{-1}; P_{LA}, 10 mmHg). After attaining the target values at around 20 min, *AP*, *CO*, and P_{LA} were maintained at these levels stably throughout stepwise changes in *HR*. *HR* was reduced from 130 to 80 bpm in 10-bpm steps. Following *HR* reduction, the regulator increased the infusion rate of DOB to maintain S_L (Fig. 3). The regulator also decreased the infusion rate of SNP, and discontinued DEX infusion, thereby maintaining *R* and *V*, respectively. After attaining the lowest *HR* (80 bpm), *HR* was increased to 100 and 130 bpm. For each *HR* step, *AP*, *CO*, and P_{LA} were precisely controlled with minimum absolute errors from target values (error in *AP*, 3 ± 1 mmHg; error in CO, 1 ± 0 mL min^{-1} · kg^{-1}; error in P_{LA}, 0.3 ± 0.1 mmHg).

TABLE 2. Hemodynamic and left ventricular mechanoenergetic data at baseline (*Baseline*), and after coronary artery embolization (*AHF*).

	Baseline	*AHF*
HR, bpm	140 ± 7	146 ± 8
AP, mmHg	114 ± 4	97 ± 5†
CO, mL min^{-1} · kg^{-1}	101 ± 5	62 ± 5†
P_{LA}, mmHg	8.9 ± 0.6	17.1 ± 0.7†
E_{es}, mmHg mL^{-1}	4.4 ± 0.7	2.5 ± 0.4*
SW, mmHg mL	1667 ± 300	933 ± 91
PVA, mmHg mL	3292 ± 302	3235 ± 515
BVO_2, μL O_2 · beat^{-1}	41 ± 5	21 ± 1†
ME, %	36 ± 4	31 ± 4
MVO_2, mL O_2 · min^{-1}	5.8 ± 0.7	3.1 ± 0.2*

*$p < 0.05$, †$p < 0.01$ vs. *Baseline*. Values are mean ± SEM. *HR*, heart rate; *AP*, systemic arterial pressure; *CO*, cardiac output; P_{LA}, left atrial pressure; E_{es}, left ventricular (LV) end-systolic elastance; *SW*, LV stroke work; *PVA*, LV pressure–volume area; BVO_2, LV oxygen consumption per beat; *ME*, LV mechanical efficiency; MVO_2, LV oxygen consumption per minute.

Figure 4 demonstrates the relations of *HR* with E_{es} (Panel a), with *SW* (Panel b), with *PVA* (Panel c), with BVO_2 (Panel d), with *ME* (Panel e), and with MVO_2 (Panel f), which were determined at each *HR* step as shown in Fig. 3. E_{es} paralleled the infusion rate of DOB; the value increased from 2.9 to 5.3 mmHg mL^{-1} with *HR* reduction from 130 to 80 mmHg, and decreased to 3.3 mmHg mL^{-1} following the recovery of *HR* to 130 mmHg (Fig. 4a). *SW*, *PVA*, and BVO_2 increased with *HR* reduction, and decreased following the recovery of *HR* (Figs. 4b–d). Following *HR* reduction, since *SW* increased (+46%) to a greater extent than BVO_2 (+10%), *ME* increased from 51 to 67%. Following the recovery of *HR*, *ME* decreased to 52% (Fig. 4e). MVO_2 decreased from 3.3 to 2.3 mL O_2 min^{-1} with *HR* reduction, and increased to 3.0 mL O_2 min^{-1} following the recovery of *HR* (Fig. 4f). These changes in LV mechanoenergetic data are reasonably compatible with those predicted in *Theoretical analysis* (Fig. 1 compared with Fig. 4).

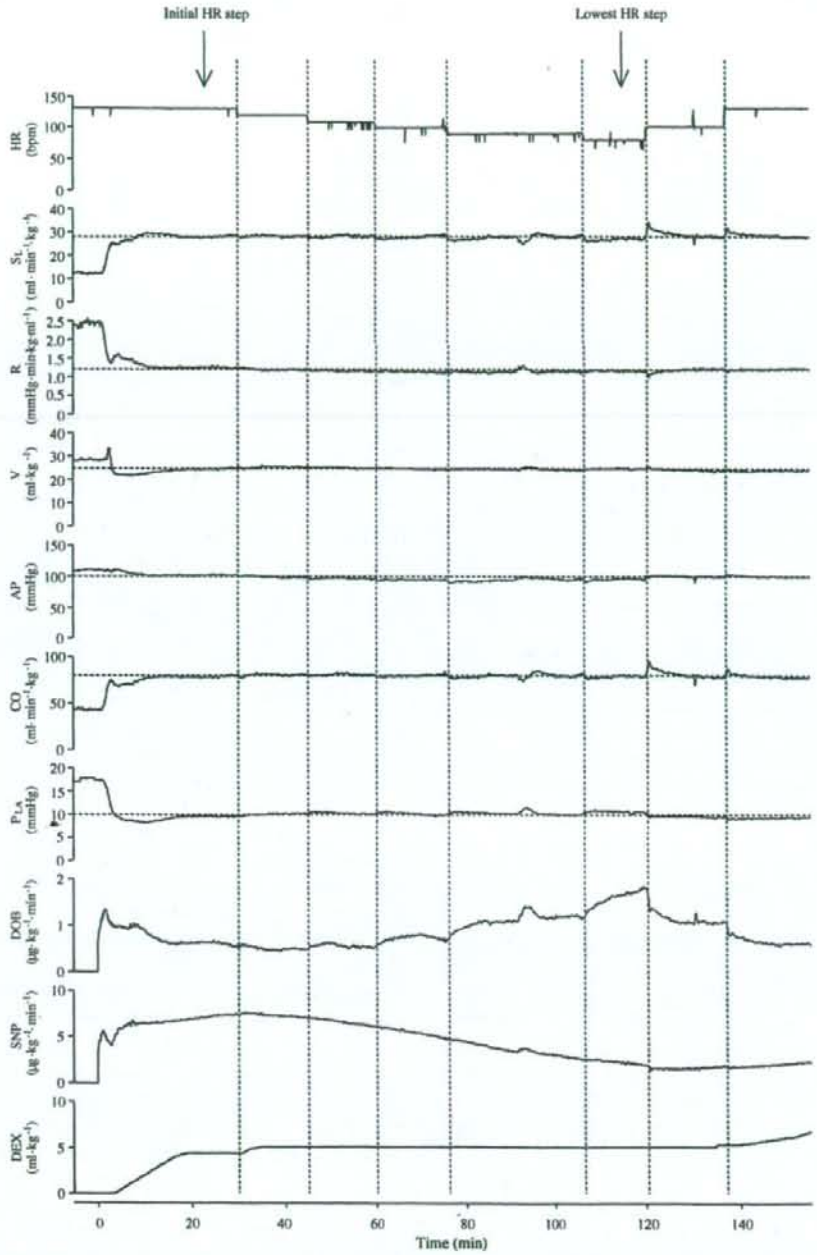

FIGURE 3. Time courses of heart rate (*HR*), S_L, *R*, *V*, *AP*, *CO*, P_{LA}, infusion rates of DOB, SNP, and accumulated volume of infused DEX in one representative animal during control of hemodynamics by the automated hemodynamic regulator. Target values of S_L, *R*, *V*, *AP*, *CO*, and P_{LA} are depicted by horizontal dotted lines in each trace. The *HR* steps (80–130 bpm) are separated by vertical dotted lines.

Table 3 summarizes the hemodynamic and drug infusion data at *AHF*, *Initial HR*, and *Lowest HR* in seven animals. In four animals, FUR (10 mg) was injected once between the *Initial HR* step and the *Lowest HR* step, and the total urine volume was 190–460 mL. Comparing the data at *Initial HR* and

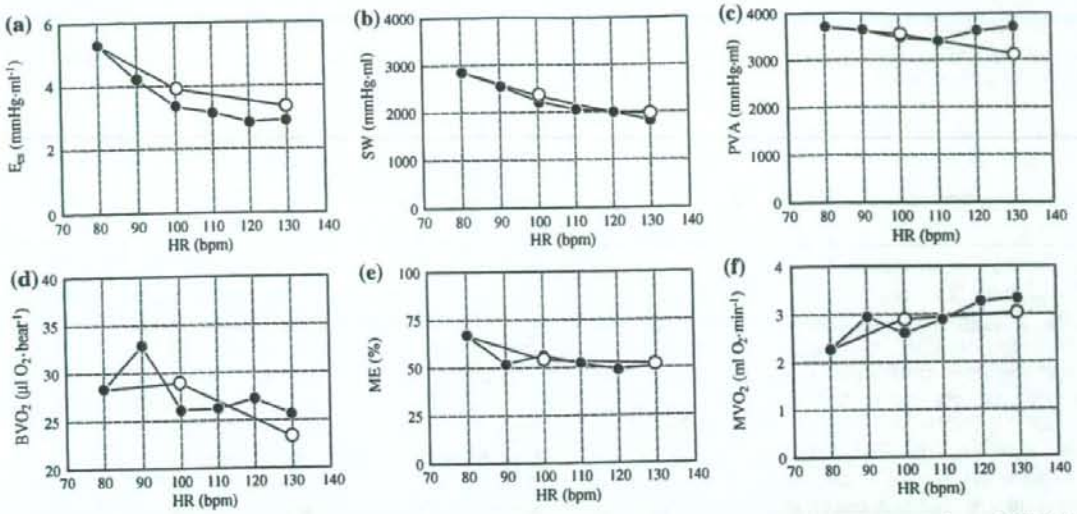

FIGURE 4. Relations of heart rate (*HR*) with left ventricular end-systolic elastance (E_{es}) (a), left ventricular stroke work (*SW*) (b), left ventricular pressure–volume area (*PVA*) (c), left ventricular oxygen consumption per beat (BVO_2) (d), left ventricular mechanical efficiency (*ME*) (e), and left ventricular oxygen consumption per minute (MVO_2) (f) determined at each *HR* step depicted in Fig. 3. •, measurement at each *HR* step while *HR* was reduced from 130 to 80 bpm; ○, measurement at each *HR* step when *HR* was increased from 100 to 130 bpm.

TABLE 3. Hemodynamic data and drug infusion rates after coronary artery embolization (*AHF*), at the initial *HR* (*Initial HR*), and at the lowest *HR* (*Lowest HR*).

	AHF	*Initial HR*	*Lowest HR*
HR, bpm	146 ± 8	146 ± 8	107 ± 7*,†
S_L, mL min^{-1} · kg^{-1}	18 ± 2	31 ± 1*	30 ± 1*
R, mmHg·min · kg · mL^{-1}	1.5 ± 0.2	1.0 ± 0.1*	1.0 ± 0.0*
V, mL · kg^{-1}	31 ± 1	27 ± 1*	27 ± 1*
DOB, μg min^{-1} kg^{-1}		1.4 ± 0.3	2.7 ± 0.5†
SNP, μg min^{-1} kg^{-1}		4.1 ± 0.8	2.4 ± 0.6
DEX, mL kg^{-1}		4.0 ± 0.7	0.8 ± 0.3†
AP, mmHg	97 ± 5	94 ± 3	93 ± 2
CO, mL min^{-1} kg^{-1}	62 ± 5	89 ± 3*	88 ± 3*
P_{LA}, mmHg	17.1 ± 0.7	10.5 ± 0.4*	10.9 ± 0.4*

*$p < 0.01$ vs. *AHF*, †$p < 0.01$ vs. *Initial HR*. Values are mean ± SEM. S_L, functional slope of the left ventricular Starling's curve; *R*, systemic vascular resistance; *V*, stressed blood volume; DOB, infusion rate of dobutamine; SNP, infusion rate of sodium nitroprusside; DEX, the value at *Initial HR* indicates the volume of dextran infused from the activation of the regulator until the *Initial HR*, the value at *Lowest HR* that from the *Initial HR* until the *Lowest HR*.

Lowest HR with those at *AHF*, S_L was increased while *R* and *V* were decreased significantly, indicating that cardiac function was improved while peripheral vasoconstriction and volume retention were relieved by our hemodynamic regulator. As a result, *CO* increased and P_{LA} decreased significantly. *AP*, *CO*, and P_{LA} were controlled precisely in all the animals with minimal absolute errors from target values (error in *AP*, 2 ± 0 mmHg; error in *CO*, 2 ± 0 mL min^{-1} kg^{-1}; error in P_{LA}, 0.4 ± 0.0 mmHg). Comparing the data at *Lowest HR* with those at *Initial HR*, HR decreased significantly (−27 ± 3%), the infusion rate of DOB increased significantly (+116 ± 23%), and the infused volume of DEX decreased significantly (−83 ± 7%).

Figure 5 summarizes the LV mechanoenergetic data at *AHF*, *Initial HR*, and *Lowest HR* in seven animals. When the data at *Initial HR* and *Lowest HR* were compared with those at *AHF*, E_{es}, *SW*, BVO_2, and *ME* increased, but *PVA* decreased significantly. MVO_2 at *Initial HR* also increased compared to that at *AHF*, although MVO_2 at *Lowest HR* was almost identical to that at *AHF*. The automated hemodynamic regulator restored normal hemodynamics with increased energy cost at *Initial HR*, but with diminished energy cost at *Lowest HR*. Comparing the data at *Lowest HR* with those at *Initial HR*, E_{es} increased significantly (+34 ± 14%), *SW* increased significantly (+37 ± 6%), and BVO_2 increased significantly (+12 ± 2%). Since *SW* increased to a greater extent than BVO_2, *ME* increased (+22 ± 6%) and MVO_2 decreased significantly (−17 ± 4%). Changes in the LV mechanoenergetic data following *HR* reduction averaged over seven animals are compatible with those predicted in *Theoretical analysis*.

DISCUSSION

To the best of our knowledge, we are the first to succeed in improving cardiac energetics without compromising normal hemodynamic conditions in acute

heart failure. Only by using our automated hemodynamic regulator, induced bradycardia improved cardiac energetic efficiency while restoring and strictly maintaining normal hemodynamic conditions in a canine model of acute heart failure.

Complicated Multiple Drug Infusions

Complicated regulations of multiple drug infusions were required to maintain *AP*, *CO*, and P_{LA} during *HR* reduction. It is difficult and unrealistic to control multiple drug infusions manually in hemodynamically unstable patients after bradycardia is induced.

Equation (1) indicates that *HR* reduction alone decreases S_L. In response to *HR* reduction, the negative feedback mechanism of our regulator automatically increases the infusion rate of DOB, which increases LV E_{es} and maintains S_L (Table 3, Fig. 5). An excessive increase in LV E_{es} can offset the MVO_2-decreasing effect of *HR* reduction. Therefore, the infusion rate of DOB must be precisely controlled. This is especially important when the oxygen cost of contractility is pathologically increased as observed in heart failure, where an oxygen-wasting effect of DOB may become crucial.[15]

DOB may increase *V*.[3] Our regulator effectively compensates the volume increasing effect of DOB by reducing or discontinuing DEX infusion, or by infusing FUR (Fig. 3, Table 3). DOB may also change *R*, and usually reduces *R*.[3] In some cases, the resistance-lowering effect of DOB is compensated by a decrease in infusion rate of SNP (Fig. 3). If these secondary effects of DOB are not adequately compensated, target hemodynamic conditions can no longer be maintained.

Comparison with Previous Hemodynamic Regulators

Apart from our automated hemodynamic regulator, several systems that automate the infusions of multiple cardiovascular drugs to control *AP* and *CO*, or *AP* and pulmonary arterial pressure have been reported.[17,23,33] However, it would be difficult to use these systems to improve the cardiac energetic efficiency. As indicated in *Theoretical analysis*, cardiac energetic efficiency is determined by *HR*, *AP*, *CO*, and P_{LA}. Those previous systems are incomplete for simultaneously control of all these multiple hemodynamic variables. Unstable performance of these systems sometimes results in drastic change of *HR*. Persistent oscillations of *CO* occurred following an abrupt increase in *HR* during automated hemodynamic control by a previously reported system.[23]

Our regulator controls the mechanical determinants of circulation, and as a result achieves target values for hemodynamic variables.[30] Previous systems[17,23,33]

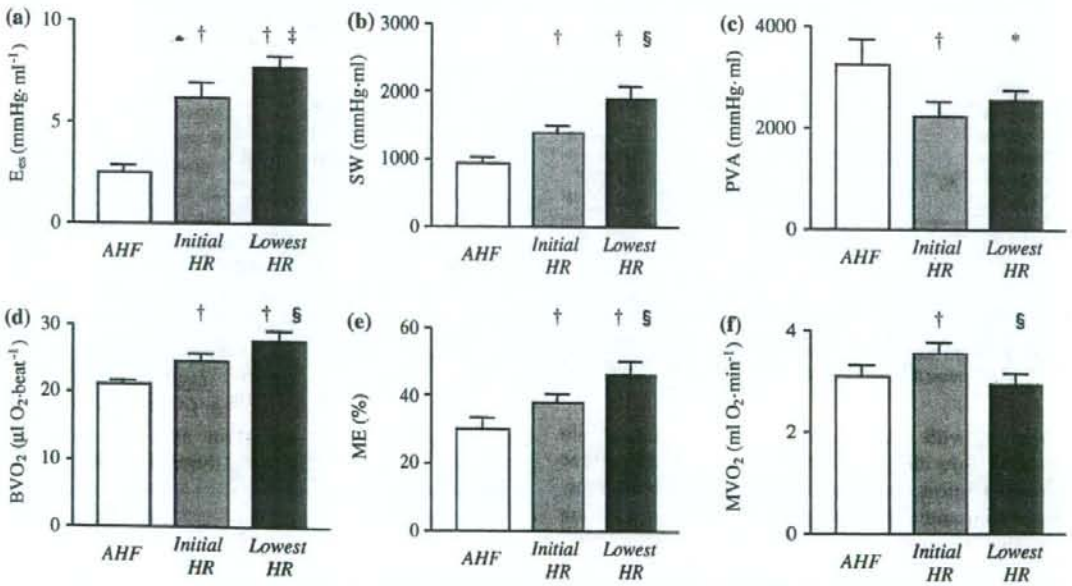

FIGURE 5. Left ventricular mechanoenergetic data after coronary artery embolization (*AHF*), at the initial *HR* (*Initial HR*), and at the lowest *HR* (*Lowest HR*). E_{es}, left ventricular (LV) end-systolic elastance; *SW*, LV stroke work; *PVA*, LV pressure–volume area; BVO_2, LV oxygen consumption per beat; *ME*, LV mechanical efficiency; MVO_2, LV oxygen consumption per minute. Data are means ± SEM. *$p<0.05$, †$p<0.01$ vs. *AHF*. ‡$p<0.05$, §$p<0.01$ vs. *Initial HR*.

attempted to control hemodynamic variables by estimating the apparent input–output relations between drug infusion and response of the controlled variables. In the systems that control *AP* and *CO*,[23,33] all possible input–output relations have to be estimated; namely, inotrope–*AP*, inotrope–*CO*, vasodilator–*AP*, and vasodilator–*CO* relations. The reason is that these drugs affect *AP* and *CO* simultaneously to almost the same degree. If this previous approach is applied to simultaneous control of *AP*, *CO*, and P_{LA}, at least 9 input–output relations have to be estimated, since at least 3 drugs are required to independently control the three variables. This would make the system extremely complicated, and therefore be practically unfeasible. The three drug controllers in our regulator (Fig. 2) are designed on the basis of only three input–output relations between drug infusion and response of the controlled parameter; namely, DOB–S_L, SNP–*R*, and DEX/FUR–*V*.[30] The fact that the three closed loops are effectively decoupled simplifies the entire system. This also permits a system operator, who would be a physician untrained in control engineering, to understand its behavior easily.

Comparison to Previous Studies on LV Mechanoenergetics

Several studies examined LV mechanoenergetics under LV inotropy and bradycardia *in vivo*.[16,25] Single drug or two-drug combinations were used and infusions were titrated manually. However, *HR* reduction inevitably induced changes in *AP*, *CO*, or P_{LA} in these studies.

Shen *et al.*[25] compared the inotropic/chronotropic effects and MVO_2 in response to the sodium channel enhancer LY341311 with those in response to dobutamine in dogs with heart failure. LY341311 increased LV dP/dt_{max} and decreased *HR*. At similar levels of inotropic response and similar levels of *AP* and P_{LA}, dobutamine increased MVO_2 whereas LY341311 did not. These results suggested a favorable effect of LY341311 on myocardial energetics. However, the investigators did not evaluate *CO*. Since left ventricular end-diastolic volume and ventricular fractional shortening were also comparable between the two groups, *CO* must be lower in the LY341311 group in proportion to the magnitude of HR reduction. The favorable effect of LY341311 on myocardial energetics might be in part at the sacrifice of *CO*, i.e., at the sacrifice of peripheral perfusion.

Absolute values of *ME* obtained in the present study (30–70%) were higher than those reported in previous studies (<30%).[19,26,28] Differences in experimental methods may be one reason for this discrepancy. We measured the coronary blood flow using the ultrasonic flow meters placed on the anterior descending and circumflex coronary arteries. However, owing to technical difficulties, blood flow in most proximal branches of the anterior descending artery, such as the first septal and/or first diagonal branches were not included. On the other hand, previous studies using coronary sinus thermo-dilution catheters[19,26] or cross-circulated dog heart preparations[28] were able to measure total coronary artery blood flow including that in proximal branches. Systematic underestimation of coronary blood flow in our study might result in systematic underestimation of ventricular oxygen consumption, and as a result overestimation of *ME*. In addition, *SW* calculated by Eq. (3) does not fully describe the net external work done by LV per cardiac cycle, since diastolic work performed on the ventricle was assessed inaccurately.[11] However, *SW* calculated by Eq. (3) and the net external work determined by the LV pressure–volume loop correlates with high linearity.[11] Taken together, it is fair to say that the direction and magnitude of changes in MVO_2 and *ME* were evaluated accurately in the present study.

Comparison with Beta-blockade Alone

The degree of reduction in MVO_2 (17%, *Lowest HR* vs. *Initial HR* in Fig. 5f) when HR was reduced by 30% in the present experiment is less than that observed in beta-blockade treatment. For example, atenolol decreased MVO_2 by 40% when *HR* was reduced by 30% in dogs during exercise.[6] Negative ventricular inotropy accompanying *HR* reduction accounts for the further reduction in MVO_2 achieved by beta-blockade.[6] However, in acute heart failure, use of beta-blockers is contraindicated owing to its adverse effects on systemic hemodynamics.[1,5] Taken together, the degree of reduction in MVO_2 obtained in this study is reasonable considering that it is achieved without sacrificing the normal hemodynamic condition.

Use of Specific Bradycardic Agent

Under physiological conditions, HR and the ventricular contractility are internally coupled, and is known as the force frequency relationship.[8] In the present study, co-administration of zatebradine with DOB uncoupled this relationship and allowed us to change *HR* and the ventricular contractility (E_{es}) in opposite directions (Fig. 4a).[24] Zatebradine selectively inhibits funny current, which is a primary sinoatrial node pacemaker current, and does not inhibit calcium channel.[12] Therefore, zatebradine reduced *HR* with little influence on the positive inotropic effect of DOB.

Zatebradine has not been further developed for clinical use. Its successor ivabradine belongs to the

same class of selective *HR*-lowering agents that act specifically on the sinoatrial node, and has been approved for clinical application.[4] The fact that ivabradine reduces *HR* dose dependently suggests that in future clinical application of our regulator, we may be able to control the *HR* reduction by titrating ivabradine infusion only without the need of atrial pacing.

Limitations

Figure 1 suggests that if heart rate is reduced beyond a critical value at which MVO_2 becomes minimal, cardiac energetics does not improve, or even deteriorates. This finding indicates that over-reduction of *HR* below the critical value should be avoided when applying the present framework to hemodynamic management. As indicated in Theoretical analysis, satisfactory management would be generally achieved in dogs if *HR* is maintained above 75 bpm. For clinical application of the present framework, a method has to be established to estimate the critical *HR* in each cardiac patient.

We directly measured *CO* and P_{LA} in open chest condition, which is not relevant to the clinical setting. Several methods have been developed to continuously monitor these variables in closed chest conditions.[2] Integrating these methods into our regulator would bring the clinical application of our regulator closer to reality.

The neurohormonal-mediated reflexes, which might have been attenuated by anesthesia in the present study, may cause unstable automated hemodynamic control under conscious condition. Patients with acute heart failure usually have a long history of cardiovascular dysfunction resulting from extensive myocardial remodeling, down-regulation of major receptors controlling HR, contractility, and myocardial oxygen metabolism.[22] This was not the case in our model as the dogs were treated with glass microspheres to induce acute heart failure. Response to our interventional strategy in a chronic heart failure model may be different from that observed in this study. Further studies on these respects are clearly required.

Although reduction in MVO_2 following HR reduction was statistically significant, the degree of reduction was rather mild (Fig. 5f). Furthermore, increase in ventricular contractility suggests that calcium transient may be increased on a single beat basis. Calcium overload closely correlates with myocardial damage and cell death.[21] Whether the improvement in myocardial energetics as achieved in the present study really ameliorates the myocardial damage in acute heart failure remains to be evaluated in future studies.

CONCLUSION

In a canine acute heart failure model, direct control of the mechanical determinants of circulation using an automated hemodynamic regulator improved cardiac energetic efficiency while restoring normal hemodynamic conditions. Our system may be a useful tool in managing hemodynamically unstable patients with acute heart failure.

APPENDIX

Feedback Control Algorithms of the Automatic Hemodynamic Regulator

To minimize the difference between target and subject's S_L (ΔS_L = target S_L—subject's S_L) and those of R (ΔR = target R—subject's R), the proportional-integral (PI) feedback controllers adjust the infusion rates of DOB and SNP, respectively (Fig. 2). In the PI controller (Fig. 6), ΔS_L (or ΔR) and the difference integrated with an integral gain (K_i) are summed and scaled by a proportional gain (K_p) to give the infusion rate of DOB (or SNP). PI gain constants for DOB infusion [$K_i = 0.01\ s^{-1}$, $K_p = 0.06\ \mu g\ kg^{-1}\ min^{-1}$ (mL $min^{-1}\ kg^{-1})^{-1}$] and for SNP infusion [$K_i = 0.007\ s^{-1}$, $K_p = -1.37\ \mu g\ kg^{-1}\ min^{-1}$ (mmHg min ml^{-1} kg)$^{-1}$] were determined on the basis of open-loop response of S_L and R to the infusion of DOB and SNP, respectively.[30]

To minimize the difference between target and subject's V (ΔV = target V—subject's V), a nonlinear (N-L) feedback controller (Fig. 2) adjusts the infusion of DEX or injection of FUR based on the following "if-then" rules:

Rule 1: If $\Delta V \geq 1$ mL kg^{-1} then infuse DEX at 10 mL min^{-1}
Rule 2: If $\Delta V \leq -2$ mL kg^{-1} then inject FUR (10 mg) at 10 min intervals

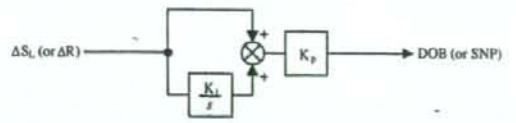

FIGURE 6. Block diagram of the PI controller in the automated hemodynamic regulator. ΔS_L and ΔR denote the difference between target and subject's S_L, and between target and subject's R, respectively. K_i and K_p represent the integral and proportional gain constants, respectively. s is a Laplace operator.

The "if-then" rules were determined on the basis of the open-loop response of V to the infusion of DEX and FUR.[30]

ACKNOWLEDGMENT

This study was supported by Grant-in-Aid for Scientific Research (C) (18500358, 20500404) from the Ministry of Education, Culture, Sports, Science and Technology, by a research grant from Nakatani Foundation of Electronic Measuring Technology Advancement, and by Health and Labour Sciences Research Grants (H19-nano-ippan-009) from the Ministry of Health, Labour and Welfare of Japan.

REFERENCES

[1]Antman, E. M., D. T. Anbe, P. W. Armstrong, E. R. Bates, L. A. Green, M. Hand, J. S. Hochman, H. M. Krumholz, F. G. Kushner, G. A. Lamas, C. J. Mullany, J. P. Ornato, D. L. Pearle, M. A. Sloan, S. C. Smith, Jr., J. S. Alpert, J. L. Anderson, D. P. Faxon, V. Fuster, R. J. Gibbons, G. Gregoratos, J. L. Halperin, L. F. Hiratzka, S. A. Hunt, A. K. Jacobs, and J. P. Ornato. American College of Cardiology; American Heart Association; Canadian Cardiovascular Society ACC/AHA guidelines for the management of patients with ST-elevation myocardial infarction–executive summary. A report of the American College of Cardiology/American Heart Association Task Force on Practice Guidelines (Writing Committee to revise the 1999 guidelines for the management of patients with acute myocardial infarction). *J. Am. Coll. Cardiol.* 44:671–719, 2004. doi:10.1016/j.jacc.2004.07.002.

[2]Bein, B., F. Worthmann, P. H. Tonner, A. Paris, M. Steinfath, and J. Hedderich. Comparison of esophageal Doppler, pulse contour analysis, and real-time pulmonary artery thermodilution for the continuous measurement of cardiac output. *J. Cardiothorac. Vasc. Anesth.* 18:185–189, 2004. doi:10.1053/j.jvca.2004.01.025.

[3]Binkley, P. F., K. D. Murray, K. M. Watson, P. D. Myerowitz, and C. V. Leier. Dobutamine increases cardiac output of the total artificial heart. Implications for vascular contribution of inotropic agents to augmented ventricular function. *Circulation* 84:1210–1215, 1991.

[4]Borer, J. S., K. Fox, P. Jaillon, and G. Lerebours. Antianginal and antiischemic effects of ivabradine, an I(f) inhibitor, in stable angina: a randomized, double-blind, multicentered, placebo-controlled trial. *Circulation* 107: 817–823, 2003. doi:10.1161/01.CIR.0000048143.25023.87.

[5]Choong, C. Y., G. S. Roubin, P. J. Harris, Y. Tokuyasu, W. F. Shen, G. J. Bautovich, and D. T. Kelly. A comparison of the effects of beta-blockers with and without intrinsic sympathomimetic activity on hemodynamics and left ventricular function at rest and during exercise in patients with coronary artery disease. *J. Cardiovasc. Pharmacol.* 8:441–448, 1986. doi:10.1097/00005344-198605000-00001.

[6]Colin, P., B. Ghaleh, X. Monnet, J. Su, L. Hittinger, J. F. Giudicelli, and A. Berdeaux. Contributions of heart rate and contractility to myocardial oxygen balance during exercise. *Am. J. Physiol. Heart Circ. Physiol.* 284:H676–H682, 2003.

[7]Colucci, W. S. Myocardial and vascular actions of milrinone. *Eur. Heart J.* 10(Suppl C):32–38, 1989.

[8]Freeman, G. L., W. C. Little, and R. A. O'Rourke. Influence of heart rate on left ventricular performance in conscious dogs. *Circ. Res.* 61:455–464, 1987.

[9]Gingrich, K. J., and R. J. Roy. Modeling the hemodynamic response to dopamine in acute heart failure. *IEEE Trans. Biomed. Eng.* 38:267–272, 1991. doi:10.1109/10.133208.

[10]Glantz, S. A. Ventricular pressure–volume curve indices change with end-diastolic pressure. *Circ. Res.* 39:772–778, 1976.

[11]Glower, D. D., J. A. Spratt, N. D. Snow, J. S. Kabas, J. W. Davis, C. O. Olsen, G. S. Tyson, D. C. Sabiston, Jr., and J. S. Rankin. Linearity of the Frank–Starling relationship in the intact heart: the concept of preload recruitable stroke work. *Circulation* 71:994–1009, 1985.

[12]Guth, B. D., and T. Dietze. If current mediates β-adrenergic enhancement of heart rate but not contractility in vivo. *Basic Res. Cardiol.* 90:192–202, 1995. doi:10.1007/BF00805662.

[13]Hamlin, R. L., T. Nakayama, H. Nakayama, and C. A. Carnes. Effects of changing heart rate on electrophysiological and hemodynamic function in the dog. *Life Sci.* 72:1919–1930, 2003. doi:10.1016/S0024-3205(03)00015-8.

[14]Hayashi, K., K. Shigemi, T. Shishido, M. Sugimachi, and K. Sunagawa. Single-beat estimation of ventricular end-systolic elastance-effective arterial elastance as an index of ventricular mechanoenergetic performance. *Anesthesiology* 92:1769–1776, 2000. doi:10.1097/00000542-200006000-00037.

[15]Hayashi, Y., M. Takeuchi, H. Takaoka, K. Hata, M. Mori, and M. Yokoyama. Alteration in energetics in patients with left ventricular dysfunction after myocardial infarction: increased oxygen cost of contractility. *Circulation* 93:932–939, 1996.

[16]Hettrick, D. A., P. S. Pagel, D. Lowe, J. P. Tessmer, and D. C. Warltier. Increases in inotropic state without change in heart rate: combined use of dobutamine and zatebradine in conscious dogs. *Eur. J. Pharmacol.* 316:237–244, 1996. doi:10.1016/S0014-2999(96)00688-7.

[17]Hoeksel, S. A., J. A. Blom, J. R. Jansen, J. G. Maessen, and J. J. Schreuder. Automated infusion of vasoactive and inotropic drugs to control arterial and pulmonary pressures during cardiac surgery. *Crit. Care Med.* 27:2792–2798, 1999. doi:10.1097/00003246-199912000-00031.

[18]Iellamo, F., J. A. Sala-Mercado, M. Ichinose, R. L. Hammond, M. Pallante, T. Ichinose, L. W. Stephenson, and D. S. O'Leary. Spontaneous baroreflex control of heart rate during exercise and muscle metaboreflex activation in heart failure. *Am. J. Physiol. Heart Circ. Physiol.* 293:H1929–H1936, 2007. doi:10.1152/ajpheart.00564.2007.

[19]Kim, I. S., H. Izawa, T. Sobue, H. Ishihara, F. Somura, T. Nishizawa, K. Nagata, M. Iwase, and M. Yokota. Prognostic value of mechanical efficiency in ambulatory patients with idiopathic dilated cardiomyopathy in sinus rhythm. *J. Am. Coll. Cardiol.* 39:1264–1268, 2002. doi:10.1016/S0735-1097(02)01775-8.

[20]Knaapen, P., T. Germans, J. Knuuti, W. J. Paulus, P. A. Dijkmans, C. P. Allaart, A. A. Lammertsma, and

F. C. Visser. Myocardial energetics and efficiency: current status of the noninvasive approach. *Circulation* 115:918–927, 2007. doi:10.1161/CIRCULATIONAHA.106.660639.

[21]Miyata, H., E. G. Lakatta, M. D. Stern, and H. S. Silverman. Relation of mitochondrial and cytosolic free calcium to cardiac myocyte recovery after exposure to anoxia. *Circ. Res.* 71:605–613, 1992.

[22]Nikolaidis, L. A., T. Hentosz, A. Doverspike, R. Huerbin, C. Stolarski, Y. T. Shen, and R. P. Shannon. Catecholamine stimulation is associated with impaired myocardial O_2 utilization in heart failure. *Cardiovasc. Res.* 53:392–404, 2002. doi:10.1016/S0008-6363(01)00490-4.

[23]Rao, R. R., B. Aufderheide, and B. W. Bequette. Experimental studies on multiple-model predictive control for automated regulation of hemodynamic variables. *IEEE Trans. Biomed. Eng.* 50:277–288, 2003. doi:10.1109/TBME.2003.808813.

[24]Schipke, J. D., Y. Harasawa, S. Sugiura, J. Alexander, Jr., and D. Burkhoff. Effect of a bradycardic agent on the isolated blood-perfused canine heart. *Cardiovasc. Drugs Ther.* 5:481–488, 1991.

[25]Shen, W., R. M. Gill, B. D. Jones, J. P. Zhang, A. K. Corbly, and M. I. Steinberg. Combined inotropic and bradycardic effects of a sodium channel enhancer in conscious dogs with heart failure: a mechanism for improved myocardial efficiency compared with dobutamine. *J. Pharmacol. Exp. Ther.* 303:673–680, 2002. doi:10.1124/jpet.303.2.673.

[26]Shinke, T., M. Takeuchi, H. Takaoka, and M. Yokoyama. Beneficial effects of heart rate reduction on cardiac mechanics and energetics in patients with left ventricular dysfunction. *Jpn. Circ. J.* 63:957–964, 1999. doi:10.1253/jcj.63.957.

[27]Smiseth, O. A., and O. D. Mjos. A reproducible and stable model of acute ischaemic left ventricular failure in dogs. *Clin. Physiol.* 2:225–239, 1982. doi:10.1111/j.1475-097X.1982.tb00027.x.

[28]Suga, H. Ventricular energetics. *Physiol. Rev.* 70:247–277, 1990.

[29]Suga, H, Y. Yasumura, T. Nozawa, S. Futaki, Y. Igarashi, and Y. Goto. Prospective prediction of O_2 consumption from pressure–volume area in dog hearts. *Am. J. Physiol.* 252:H1258–H1264, 1987.

[30]Uemura, K., A. Kamiya, I. Hidaka, T. Kawada, S. Shimizu, T. Shishido, M. Yoshizawa, M. Sugimachi, and K. Sunagawa. Automated drug delivery system to control systemic arterial pressure, cardiac output, and left heart filling pressure in acute decompensated heart failure. *J. Appl. Physiol.* 100:1278–1286, 2006. doi:10.1152/japplphysiol.01206.2005.

[31]Uemura, K., T. Kawada, A. Kamiya, T. Aiba, I. Hidaka, K. Sunagawa, and M. Sugimachi. Prediction of circulatory equilibrium in response to changes in stressed blood volume. *Am. J. Physiol. Heart Circ. Physiol.* 289:H301–H307, 2005. doi:10.1152/ajpheart.01237.2004.

[32]Uemura, K., M. Sugimachi, T. Kawada, A. Kamiya, Y. Jin, K. Kashihara, and K. Sunagawa. A novel framework of circulatory equilibrium. *Am. J. Physiol. Heart Circ. Physiol.* 286:H2376–H2385, 2004. doi:10.1152/ajpheart.00654.2003.

[33]Yu, C., R. J. Roy, H. Kaufman, and B. W. Bequette. Multiple-model adaptive predictive control of mean arterial pressure and cardiac output. *IEEE Trans. Biomed. Eng.* 39:765–778, 1992. doi:10.1109/10.148385.

Annals of Biomedical Engineering, Vol. 37, No. 1, January 2009 (© 2008) pp. 112–128
DOI: 10.1007/s10439-008-9599-4

Wavelet-Based System Identification of Short-Term Dynamic Characteristics of Arterial Baroreflex

KOJI KASHIHARA,[1,2] TORU KAWADA,[3] MASARU SUGIMACHI,[3] and KENJI SUNAGAWA[4]

[1]Hypertension and Stroke Research Laboratory, Royal North Shore Hospital, University of Sydney, Ground Floor, Building 10, Royal North Shore Hospital, St. Leonards, NSW 2065, Australia; [2]National Institute for Longevity Sciences, NCGG, 36-3 Gengo, Morioka-machi, Obu City, Aichi 474-8511, Japan; [3]Department of Cardiovascular Dynamics, National Cardiovascular Center Research Institute, 5-7-1 Fujishirodai, Suita, Osaka 565-8565, Japan; and [4]Department of Cardiovascular Medicine, Kyushu University, 3-1-1, Maidashi, Higashi-ku, Fukuoka 812-8582, Japan

(Received 1 February 2008; accepted 31 October 2008; published online 12 November 2008)

Abstract—The assessment of arterial baroreflex function in cardiovascular diseases requires quantitative evaluation of dynamic and static baroreflex properties because of the frequent modulation of baroreflex properties with unstable hemodynamics. The purpose of this study was to identify the dynamic baroreflex properties from transient changes of step pressure inputs with background noise during a short-duration baroreflex test in anesthetized rabbits with isolated carotid sinuses, using a modified wavelet-based time-frequency analysis. The proposed analysis was able to identify the transfer function of baroreflex as well as static properties from the transient input-output responses under normal [gain at 0.04 Hz from carotid sinus pressure (CSP) to arterial pressure ($n = 8$), 0.29 ± 0.05 at low (40–60 mmHg), 1.28 ± 0.12 at middle (80–100 mmHg), and 0.38 ± 0.07 at high (120–140 mmHg) CSP changes] and pathophysiological [gain in control vs. phenylbiguanide ($n = 8$); 0.32 ± 0.07 vs. 0.39 ± 0.09 at low, 1.39 ± 0.15 vs. 0.59 ± 0.09 ($p < 0.01$) at middle, and 0.35 ± 0.04 vs. 0.15 ± 0.02 ($p < 0.01$) at high CSP changes] conditions. Subsequently, we tested the proposed wavelet-based method under closed-loop baroreflex responses; the simulation study indicates that it may be applicable to clinical situations for accurate assessment of dynamic baroreflex function. In conclusion, the dynamic baroreflex property to various pressure inputs could be simultaneously extracted from the step responses with background noise.

Keywords—Baroreceptor reflex, Sympathetic nerve activity, Arterial pressure, Transfer function, Dynamic characteristics.

INTRODUCTION

Arterial baroreflex is a crucial negative feedback system because of the quick stabilization of arterial pressure (AP) against external pressure disturbances.[12,30] The assessment of arterial baroreflex function would require quantifying the dynamic as well as static properties[15,46] because the baroreflex gain or sensitivity is frequently modulated during cardiovascular diseases.[6,36,39] Because quick responses of autonomic nerves and AP mainly through the brainstem[3] might contain the unknown characteristics changing by the minute in acute cardiovascular diseases,[25] the short-term dynamic system identification might relate to the novel finding under such nonstationary condition. Laboratory and spontaneous baroreflex methods[37] are widely used in human and animal studies. The laboratory method requires invasive pharmacological or mechanical pressure interventions, and it may be suitable for estimation of the mechanism of AP regulation through the sympathetic as well as vagal baroreflex.[7,45] The spontaneous baroreflex method aims to assess cardiovagal activity noninvasively using systolic AP and heart rate variability.[5] These methods have various merits under the baroreflex testing conditions, but remain debatable because of complicated mechanisms.[27,37,40,43]

In the laboratory method, the standard analysis of sympathetic baroreflex has been performed mainly in the time[10,16] or frequency domain.[1,29,35,44] The time-domain analysis has evaluated the stable or maximal gain around the operating point, but may not characterize the impaired dynamic baroreflex properties accurately in cardiovascular patients with unstable hemodynamics and background noise. In the frequency domain, fast Fourier transform (FFT) analysis[31] has identified dynamic baroreflex properties under such noisy condition, but requires longer data segments to cancel the background noise and to identify the dynamic properties with low-frequency band,[38] indicating difficulties to extract short-term changes. In

Address correspondence to Koji Kashihara, Hypertension and Stroke Research Laboratory, Royal North Shore Hospital, University of Sydney, Ground Floor, Building 10, Royal North Shore Hospital, St. Leonards, NSW 2065, Australia. Electronic mail: kojikasi-nils@umin.ac.jp

the spontaneous baroreflex method, the analytical time window based on short-time FFT[5] (STFFT) has been adjusted to evaluate the time-varying gain around the operating point. However, this method may not be suitable for the evaluation of short-term changes in baroreflex properties for AP regulation through sympathetic as well as vagal nerves, at multiple pressure points with background noise. A combination of time and frequency analysis using wavelet transform may be able to identify the dynamic baroreflex properties efficiently regardless of background noise[2,4] by virtue of its high temporal resolution.[34] If dynamic and static characteristics in cardiovascular patients with unstable hemodynamics can be identified in a short-duration baroreflex test, various pathophysiological characteristics may be gained simultaneously.

The first purpose of this study was to examine whether a proposed wavelet-based time-frequency analysis was able to identify the dynamic as well as static baroreflex properties in animals from transient step pressure inputs with background noise during a short-duration test. Next, the proposed analysis was applied to identify unknown dynamic baroreflex properties in nonlinear AP input ranges during the Bezold-Jarisch reflex (BJR). We hypothesized that the proposed analysis could evaluate the baroreflex transfer properties from a short-term protocol, simultaneously at various pressure inputs under normal and BJR conditions. Finally, we examined the possibility of applying the new analysis to human studies to evaluate the dynamic baroreflex for AP regulation through the sympathovagal activity.

METHODS

Pathways of Baroreflex Functions

Under the carotid sinus open-loop condition, we defined the total loop as the system from carotid sinus pressure (CSP) input to AP output, which is divided into the neural arc as the subsystem from CSP input to renal sympathetic nerve activities (RSNA) output and the peripheral arc as the subsystem from RSNA input to AP output.[15] The cardiac baroreflex was defined as the system from CSP to heart rate (HR) response,[52] which may represent sympathovagal control of the heart through the baroreflex.

Surgical Preparations

Animals were cared for in accordance with the *Guiding Principles for the Care and Use of Animals in the Field of Physiological Sciences* approved by the Physiological Society of Japan. Japanese white rabbits were anesthetized with an intravenous injection (2 mL/kg) of a mixture of urethane (250 mg/mL) and α-chloralose (40 mg/mL) followed by a continuous administration (0.2–0.3 mL/kg/h, i.v.). The rabbits were artificially ventilated with oxygen-enriched room air at 0.6 Hz. Raw wave of AP was measured from the right femoral artery, using a high-fidelity pressure transducer (Millar Instruments, Houston, TX). A double-lumen catheter was placed into the right femoral vein for drug administration. The aortic depressor nerves identified by arterial pulse-synchronous activities were sectioned, while bilateral vagi were kept intact. Bilateral carotid sinuses were isolated from the systemic circulation by ligating the external and internal carotid arteries, and were filled with warm physiological saline through catheters inserted into the common carotid arteries. CSP was adjusted with a servo-controlled piston pump controlled by a computer system.

The left renal sympathetic nerve was exposed and a pair of stainless steel wire electrodes (Bioflex wire AS633, Cooner Wire) was attached. The nerve fibers distal to the electrodes were crushed by tight ligature to eliminate afferent signals from the kidney, and were covered in silicone gel (Semicosil 932A/B, Wacker Silicones). The preamplified nerve signal, band-pass filtered at 150–1000 Hz, was full-wave rectified and low-pass filtered at a cutoff frequency of 30 Hz (i.e. Op-amp RC integrator) to quantify nerve activity. Pancuronium bromide (0.3 mg/kg, i.v.) was administered to prevent muscular activity. The body temperature was kept at 38 °C.

Step Input Protocol

The carotid sinus baroreflex negative feedback loop was closed by adjusting CSP to AP level for 20 min after the surgical preparations (8 rabbits weighing 2.7–3.0 kg). The feedback loop was then opened and CSP was maintained at 40 mmHg for 4 min until the AP response reached a steady state. CSP was then increased from 40 to 160 mmHg in increments of 20 mmHg every minute (CSP_{40-60}, CSP_{60-80}, CSP_{80-100}, $CSP_{100-120}$, $CSP_{120-140}$, and $CSP_{140-160}$ changes). The single trial was repeated three times every rabbit. Data were sampled at 200 Hz and were averaged every 40 points for analysis (i.e. pulsatile AP signals were averaged every 0.2 s). HR (beats/min) was counted from the pulse waves of raw AP signals, which are well known as waves synchronized with ECG.[33] RSNA data of each animal were presented in arbitrary units (a.u.), with 1-min averaged background noise taken as zero level and 10-s averaged RSNA at CSP of 40 mmHg in normal condition set as unity.

Data Analysis

Identification of Dynamic Baroreflex

After the recorded data (three times) of CSP, RSNA, AP and HR were averaged in each animal, the signals were convoluted by complex Morlet wavelet, $w(t, f_0)$:[48,49]

$$w(t, f_0) = \frac{1}{\sqrt{\sigma_t\sqrt{\pi}}} \cdot \exp\left(\frac{-t^2}{2\sigma_t^2}\right) \cdot \exp(2\pi f_0 it) \quad (1)$$

where the $(\sigma_t\sqrt{\pi})^{-1/2}$ normalizes the wavelets to be unity total energy, and the $\exp(-t^2/2\sigma_t^2)$ is a Gaussian shape with the central frequency f_0 at time t. The standard deviation (σ_t) of the time domain is inversely proportional to the standard deviation (σ_f) of the frequency domain [$\sigma_f = (2\pi\sigma_t)^{-1}$]. A constant ratio, f_0/σ_f, determines the effective number of oscillation cycles in the wavelet. The f_0/σ_f was determined[11] as 5 with f_0 ranging from 0.04 to 0.4 Hz[32] in increments of 0.01 Hz. Because the dynamic baroreflex function was well characterized by the transfer function up to around 0.4 Hz based on the corner frequency and slope of gain change,[15,32] the upper frequency limit for analysis was set at 0.4 Hz, considering also the limitation of the step input (low power in high frequency components) and the respiratory frequency of 0.6 Hz. The wavelet duration ($2\sigma_t$) is 39.8 s at 0.04 Hz and 3.98 s at 0.4 Hz, and the spectral band width ($2\sigma_f$) is 0.016 Hz at 0.04 Hz and 0.16 Hz at 0.4 Hz.

The linear trend was subtracted only in animal study, and the continuous wavelet transform of time series $u(t)$ was calculated as the convolution of a complex wavelet [$w(t, f_0)$] with the $u(t)$:

$$\tilde{u}(t, f_0) = w(t, f_0) * u(t) \quad (2)$$

The power $P(t, f_0)$ of the signal in a frequency band at around f_0 is the squared norm of the wavelet transform: $P(t, f_0) = |\tilde{u}(t, f_0)|^2$. The symbol (*) shows the convolution in the time domain

To identify the dynamic baroreflex property from time-sequential data, we define the transfer function [$H(t, f_0)$] from input to output using wavelet transform as follows.

$$H(t, f_0) = \frac{P_{xy}(t, f_0)}{P_{xx}(t_{event}, f_0)} \quad (3)$$

where

$$\begin{cases} P_{xx}(t_{event}, f_0) = \tilde{x}(t_{event}, f_0) \cdot \tilde{x}^{\oplus}(t_{event}, f_0) \\ P_{xy}(t, f_0) = \tilde{x}(t_{event}, f_0) \cdot \tilde{y}^{\oplus}(t, f_0) \end{cases}$$

$P_{xx}(t_{event}, f_0)$ is the auto-wavelet spectrum of the input signal [$x(t)$] with central frequency f_0 at a fixed time t_{event} when the power is maximum. The t_{event} shows the sole value of the analysis time (t) at f_0; the transfer function shows the effect of the maximum input power at t_{event} on the output responses during analysis time, t, for every f_0. Here, we used the fixed input value to extract the dynamics strictly against the step input. The cross-wavelet spectrum, $P_{xy}(t, f_0)$, which is an effective way to detect large-amplitude time-localized events,[26] is the convolution of the wavelet transform values of the input-output signals [$\tilde{x}(t_{event}, f_0)$ and $\tilde{y}^{\oplus}(t, f_0)$]. $\tilde{x}^{\oplus}(t_{event}, f_0)$ and $\tilde{y}^{\oplus}(t, f_0)$ is the complex conjugate of $x(t_{event}, f_0)$ and $y(t, f_0)$. The segment for wavelet transform analysis was set at ±30 s of the time of the step input change and was moved to the next area of the step input. The symbol (·) shows the product in the frequency domain, which corresponds to the convolution in the time domain.

To visualize the time-series transfer function during the analysis time (t), the dynamic gain $[|H(t, f_0)| = \sqrt{H_{Re}(t, f_0)^2 + H_{Im}(t, f_0)^2}$, where $H_{Re}(t, f_0)$ and $H_{Im}(t, f_0)$ are the real and imaginary parts of $H(t, f_0)$] and phase $\left[\varphi(t, f_0) = \tan^{-1}\frac{H_{Im}(t, f_0)}{H_{Re}(t, f_0)}\right]$ of the transient transfer function during analysis time were calculated from Eq. (3).

Next, we constructed the bode plot using the maximum dynamic gains, which reflects the maximum values of input and output powers. The phase of Eq. (3) is based on the maximum $P_{xx}(t_{event}, f_0)$ as the auto-wavelet spectrum of the input signal without the lag time of system response. To calculate the phase of the bode plot, we estimated the lag time of the system response as follows:

$$\hat{L} = t_{Pxy\max} - t_{Pxx\max}, \quad (4)$$

where $\hat{L}$ is the mean value between 0.35 and 0.4 Hz of f_0. The data between 0.35 and 0.4 Hz (5 points) were averaged because of the varied estimation. The analysis time was set to 0–6 s and the phase unwrap process to make it continuous across 2π phase discontinuities by adding multiples of $\pm 2\pi$ was applied. $t_{Pxx\max}$ is the time at the maximum auto power spectrum of the input data; $t_{Pxy\max}$ is the time at the maximum cross power spectrum of input-output data. Using the estimated lag time (L) of the system response, the phase [$\varphi(t_{max}, f_0)$] of the transient transfer function is shown as follows:

$$\varphi(t_{max}, f_0) = \tan^{-1}\frac{H'_{Im}(t_{max}, f_0)}{H'_{Re}(t_{max}, f_0)} \quad (5)$$

where

$$H'(t_{max}, f_0) = H(t_{max}, f_0) \cdot \exp(-2\pi f_0 iL)$$